Sixth-order magnetic moment of the electron*

Predrag Cvitanović
Laboratory of Nuclear Studies, Cornell University, Ithaca, New York 14853
and Stanford Linear Accelerator Center, Stanford University, Stanford, California 94305

T. Kinoshita†
Laboratory of Nuclear Studies, Cornell University, Ithaca, New York 14853
(Received 20 May 1974)

We have evaluated the contribution of 50 Feynman diagrams of three-photon-exchange type to the electron magnetic moment by two independent methods. The results are mutually consistent and are several times more accurate than previously reported calculations. If we combine the analytic result of Levine and Roskies for 10 diagrams and our numerical result for the remaining 40 diagrams, we obtain the best estimate available at present: $(0.922 \pm 0.024) \times (\alpha/\pi)^3$. Including the contribution from the remaining 22 diagrams calculated previously, the complete theoretical prediction for the electron anomaly up to the order α^3 is $\frac{1}{2}\alpha/\pi - 0.328\,48(\alpha/\pi)^2 + (1.195 \pm 0.026)(\alpha/\pi)^3$, in fair agreement with the latest experimental result.

I. INTRODUCTION AND SUMMARY

One of us (T.K.) has been involved for nearly eight years in an extensive program of evaluating all sixth-order Feynman integrals contributing to the electron magnetic moment (72 diagrams) and the muon magnetic moment (96 diagrams).[1-3] This article is a detailed account of the final phase of this program, i.e., the evaluation of 50 diagrams of three-photon-exchange type. A preliminary report of this work has been published two years ago.[4] Since then, however, we have developed a more satisfactory scheme for handling infrared divergences. Hence the approach of this article is somewhat different from that of Ref. 4. For this reason we have evaluated all integrals from scratch again obtaining results completely independent of the preliminary result.

For reference's sake let us classify the 72 diagrams contributing to the electron moment into four groups according to the way the vacuum-polarization subdiagrams appear in them.

Group 1: Diagrams containing fourth-order vacuum-polarization subdiagram. Four diagrams belong to this group. A typical one is shown in Fig. 1(a).

Group 2: Diagrams containing second-order vacuum-polarization subdiagram. Twelve diagrams belong to this group. A typical diagram is shown in Fig. 1(b).

Group 3: Diagrams containing photon-photon scattering subdiagram. Six diagrams belong to this group. One is shown in Fig. 1(c).

Group 4: Diagrams that contain no vacuum-polarization subdiagram. This group will be referred to as three-photon-exchange diagrams. It consists of 50 diagrams, of which 22 can be obtained from others by time reversal. A typical diagram is shown in Fig. 1(d). All distinct diagrams of this group are shown in Fig. 2.

In this paper we report on two independent calculations of $a_4^{(6)}$, the group-4 contribution to the electron anomaly. In the first approach (see Sec. V) we evaluate the diagrams of group 4 separately and combine the results afterwards. In the second approach (see Sec. VI) we classify the 50 diagrams into 10 subgroups, each consisting of five diagrams obtained by insertion of an external magnetic field vertex in one of the self-energy diagrams shown in Fig. 3, and use the Ward-Takahashi identity to handle the contribution of each subgroup as a single integral.

To set up the Feynman integrals we have made an extensive use of Feynman-Dyson rules in parametric space described in Ref. 5, hereafter referred to as I.

Most integrals thus constructed have ultraviolet (UV) and/or infrared (IR) divergences that must be subtracted or separated out before they are put on the computer. This is carried out systematically by the technique described in Ref. 6, hereafter referred to as II. Numerical integration of the resulting integrals (having five to seven integration variables) is then performed using the integration routine RIWIAD written by Lautrup, Sheppey, and Dufner.[7]

The results of numerical evaluation of individual integrals are summarized in Table I. Values of fourth-order integrals needed to obtain the contribution $a_4^{(6)}$ of group-4 diagrams of Fig. 2 to the electron anomaly are given in Table II. Combining these results we obtain the result (5.43). The numerical results of our second approach based on the self-energy diagrams of Fig. 3 are shown in

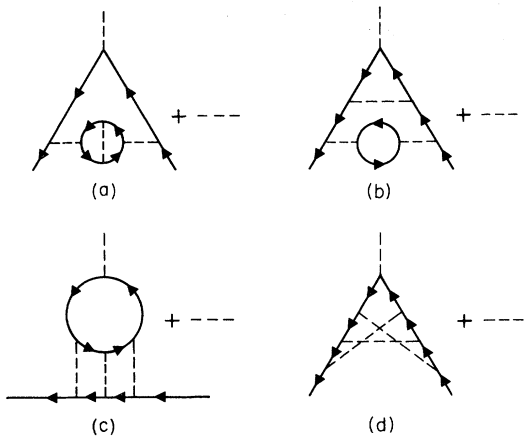

FIG. 1. (a) A typical diagram containing fourth-order vacuum-polarization subdiagram. There are three more diagrams of this type. (b) A typical diagram containing second-order vacuum-polarization subdiagram. There are 12 diagrams of this type. (c) A typical diagram containing photon-photon scattering subdiagram. Six diagrams belong to this group. (d) A typical diagram of three-photon-exchange type. There are 50 diagrams of this type.

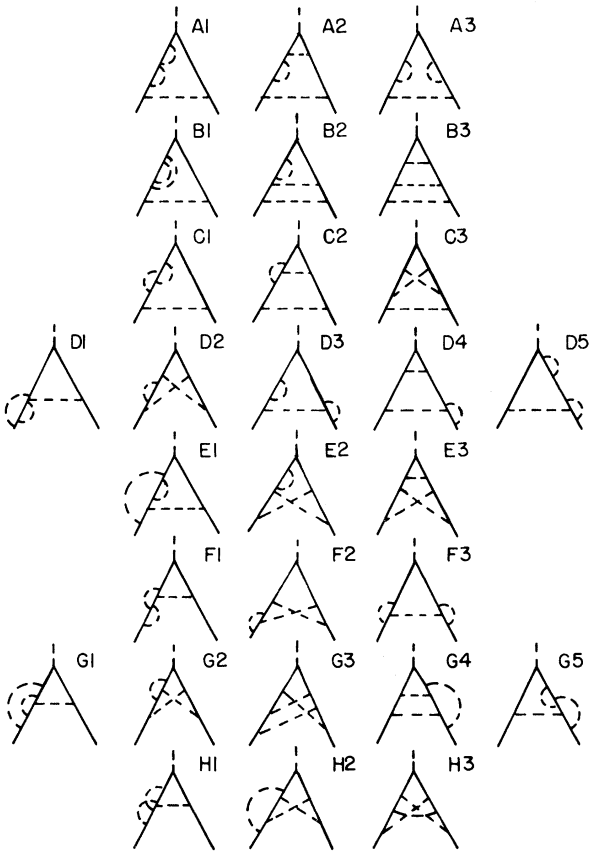

FIG. 2. 28 distinct diagrams of group 4. The remaining 22 diagrams can be obtained by time reversal.

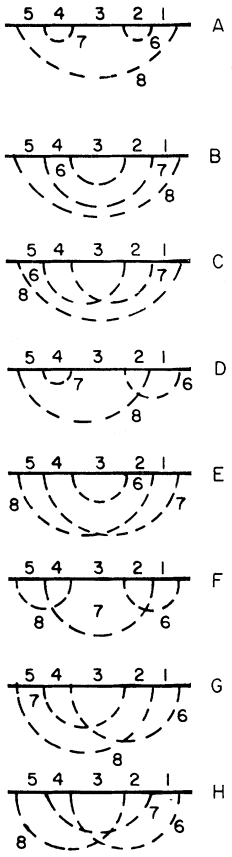

FIG. 3. Three-photon-exchange electron self-energy diagrams.

Table III. Together with the fourth-order integrals of Table II they yield the result (6.29). The uncertainties in Tables I, II, and III represent the 90% confidence limits estimated by the integration routine.

The results (5.43) and (6.29) are in good agreement with each other. However, both are outside the error limits quoted in our preliminary report.[4] Although we have not compared them in detail because of different treatments of IR-divergent terms, it is plausible that the discrepancy is primarily due to the overoptimistic treatment of errors in our preliminary calculation. See Sec. VII for details.

Recently 10 diagrams belonging to the groups A and B have been evaluated analytically.[8,9] The agreement with the numerical results is very good, assuring the soundness of the numerical approach. Until analytic evaluations of the remaining diagrams become available, the best estimate of $a_4^{(6)}$ is obtained by combining the analytic result for the diagrams of groups A and B and the weighted average of our two numerical results for groups

C, D, E, F, G, and H. This yields our final result

$$a_4^{(6)} = 0.922(24) \ . \qquad (1.1)$$

Here, in order to reduce the danger of underestimating the statistical errors, we have chosen the error in a way different from others: It is constructed by combining the smaller of two errors in each group, instead of using their statistical averages. Presumably some of the systematic errors that might be present in the RIWIAD itself are also taken care of in (1.1). As is seen from Table IV, the diagrams of group D are the major source of uncertainty in (1.1).

At present there are two other published values for $a_4^{(6)}$ (see also Ref. 10)

$$a_4^{(6)} = 0.943(60) \quad \text{(Ref. 11)}, \qquad (1.2)$$

$$a_4^{(6)} = 0.74(6) \quad \text{(Ref. 12)}. \qquad (1.3)$$

To establish the value of $a_4^{(6)}$ beyond any doubt, it is essential to compare all different calculations in detail. In Table IV we compare our two calculations. Furthermore, in Table V we give a detailed comparison of our first calculation (Sec. VII) with Refs. 8 and 11. In spite of the vastly different

TABLE I. Contributions of individual sixth-order diagrams (factor 2 included for asymmetric diagrams).

Diagram	$\eta_i \Delta M_i$	Finite parts	IR-divergent parts
$A3$	−3.1985(62)	$-2\Delta B_2 \Delta M_s + (\Delta B_2)^2 M_2$	$+2I_2(\Delta M_s - \Delta B_2 M_2) + I_2^2 M_2$
$D3$	6.0858(104)	$-2\Delta B_2 \Delta M_c$	$+2I_2(\Delta M_c - \Delta M_s + \Delta B_2 M_2) - 2I_2^2 M_2$
$F3$	−2.6564(58)		$-2I_2 \Delta M_c + I_2^2 M_2$
$A1$	−2.1232(20)	$-4\Delta B_2 \Delta M_s + 2(\Delta B_2)^2 M_2$	$+4I_2(\Delta M_s - \Delta B_2 M_2) + 2I_2^2 M_2$
$B1$	0.6918(16)	$-2\Delta B_2 \Delta M_s + 2(\Delta B_2)^2 M_2$ $-2(\Delta \delta m_b + \Delta B_b) M_2$	$+2I_2(\Delta M_s - 3\Delta B_2 M_2) + 2I_2^2 M_2 + 2(2I_s + I_l) M_2$
$C1$	−0.1708(16)	$-2(\Delta \delta m_a + \Delta B_a) M_2$	$-4I_2(\Delta M_s - \Delta B_2 M_2) - 4I_2^2 M_2 + 2(2I_c + I_x) M_2$
$D1$	1.7824(54)	$-2\Delta B_2 \Delta M_c - 2\Delta L_s M_2$	$+2I_2(\Delta M_c + \Delta B_2 M_2) - 2I_2^2 M_2 - 2I_s M_2$
$D5$	−0.5360(36)	$-2\Delta B_2 \Delta M_c$	$+2I_2(\Delta M_c - \Delta M_s + \Delta B_2 M_2) - 2I_2^2 M_2$
$E1$	1.7502(34)	$-2\Delta B_2 \Delta M_c - 2\Delta L_s M_2$	$+2I_2(\Delta M_c + \Delta B_2 M_2) - 2I_2^2 M_2 - 2I_s M_2$
$F1$	−0.9118(58)	$-2\Delta L_c M_2$	$-2I_2 \Delta M_c + 2I_2^2 M_2 - 2I_c M_2$
$G1$	0.5888(16)	$-2\Delta L_l M_2$	$-2I_2 \Delta M_c + 2I_2^2 M_2 - 2I_l M_2$
$G5$	0.9092(58)	$-2\Delta L_c M_2$	$-2I_2 \Delta M_c + 2I_2^2 M_2 - 2I_c M_2$
$H1$	−0.4218(22)	$-2\Delta L_x M_2$	$-2I_x M_2$
$A2$	3.5280(48)	$-2\Delta B_2 \Delta M_l$	$+2I_2(\Delta M_l - \Delta M_s) + 2I_s M_2$
$B2$	−0.8774(28)	$-2\Delta B_2 \Delta M_l - 2\Delta L_s M_2$	$+2I_2(\Delta M_l + \Delta M_s) - 2I_s M_2$
$C2$	2.0714(34)	$-2\Delta L_c M_2$	$+2I_2(\Delta M_c - \Delta M_l) - 2I_c M_2$
$D2$	−3.4932(96)	$-2\Delta B_2 M_x$	$+2I_2 M_x$
$D4$	−2.3774(78)		$-2I_2(\Delta M_c + \Delta M_l) + 2I_c M_2$
$E2$	0.3212(72)	$-2\Delta B_2 M_x$	$+2I_2 M_x$
$F2$	4.3184(136)		$-2I_2 M_x$
$G2$	−0.5596(34)		$-2I_2 M_x$
$G4$	−0.3182(72)		
$H2$	−1.7464(76)		
$B3$	1.8491(50)	$-\Delta L_l M_2$	
$C3$	−2.1950(58)	$-\Delta L_x M_2$	$+I_2 M_x - I_x M_2$
$E3$	−1.2157(33)		$-I_2 M_x + I_x M_2$
$G3$	1.8572(86)		
$H3$	−0.0307(27)		

TABLE II. Finite parts of renormalization counterterms.

Term	Value	Defining equation
M_2	0.5	(5.3)
ΔB_2	0.75	(3.26)
M_x	−0.4677	(5.17)
ΔM_c	0.3430	(5.17)
ΔM_l	0.7775	(5.11)
ΔM_s	−0.2950	(5.17)
ΔM_a	0.2183	(6.28)
ΔM_b	−0.1875	(6.28)
ΔL_x	−0.4796(25)	(4.29)
ΔL_c	−0.0007(18)	(4.33)
ΔL_l	0.1236(8)	(4.61)
ΔL_s	0.4070(10)	(4.58)
ΔB_a	−0.0317(44)	(4.43)
ΔB_b	−0.3946(39)	(4.67)
$\Delta\delta m_a$	−0.3015(10)	(4.6), (5.40)
$\Delta\delta m_b$	2.2059(29)	(4.48), (5.40)
$3(\Delta L_x + 2\Delta L_c) + 2\Delta\delta m_a + 2\Delta B_a$	−2.1055(22)	(5.41)
$3(\Delta L_l + 2\Delta L_s) + 2\Delta\delta m_b + 2\Delta B_b$	6.4410(5)	(5.41)
$2(\Delta L_x + 2\Delta L_c) + 2\Delta\delta m_a + \Delta B_a$	−1.5928(19)	(6.26)
$2(\Delta L_l + 2\Delta L_s) + 2\Delta\delta m_b + \Delta B_b$	5.8991(4)	(6.26)

approaches, the agreement among all these calculations is in fact very good.

For completeness we list the results for other groups:

Group 1:

$$a_1^{(6)} = \begin{cases} 0.055\,429 & \text{(Ref. 13)}, \\ 0.055\,46(6) & \text{(Ref. 3)}, \\ 0.055(2) & \text{(Ref. 14)}; \end{cases} \tag{1.4}$$

Group 2:

$$a_2^{(6)} = \begin{cases} -0.150\,17 & \text{(Ref. 15)}, \\ -0.153(5) & \text{(Ref. 3)}, \\ -0.151(3) & \text{(Ref. 14)}; \end{cases} \tag{1.5}$$

Group 3:

$$a_3^{(6)} = \begin{cases} 0.36(4) & \text{(Ref. 2)}, \\ 0.366(10) & \text{(Ref. 16)}, \\ 0.370(13) & \text{(Ref. 17)}. \end{cases} \tag{1.6}$$

The values of Ref. 13 and Ref. 15 have been obtained analytically.

The overall result for the electron anomaly up to the order α^3 is thus

$$a^{\text{th}} = \frac{1}{2}\frac{\alpha}{\pi} - 0.328\,48\left(\frac{\alpha}{\pi}\right)^2 + (1.195 \pm 0.026)\left(\frac{\alpha}{\pi}\right)^3, \tag{1.7}$$

where we have used the analytic results in (1.4), (1.5), the weighted average of the results in (1.6), and the result (1.1). If we use the ac Josephson value of the fine-structure constant[18]

$$\alpha^{-1} = 137.036\,08(26) \tag{1.8}$$

TABLE III. Contributions of grouped diagrams of sixth order (factor 2 included for asymmetric diagrams).

Group	$\eta_i \Delta M_i$	Finite parts	IR-divergent parts
A	−1.3546(52)	$-2\Delta B_2\Delta M_b + (\Delta B_2)^2 M_2$	$+2I_2(\Delta M_b - 2\Delta B_2 M_2) + 3I_2^2 M_2 + 2I_s M_2$
B	0.7920(312)	$-\Delta B_2\Delta M_b + (\Delta B_2)^2 M_2$	$+2I_2(\Delta M_b - 2\Delta B_2 M_2) + 2I_2^2 M_2$
		$-(2\Delta\delta m_b + \Delta B_b)M_2$	$+2(I_s + I_l)M_2$
C	−0.0350(97)	$-(2\Delta\delta m_a + \Delta B_a)M_2$	$+I_2(\Delta M_a - 2\Delta M_b + 2\Delta B_2 M_2) - 4I_2^2 M_2$
			$+2(2I_c + I_x)M_2$
D	0.9334(201)	$-2\Delta B_2\Delta M_a - 2\Delta L_s M_2$	$+2I_2(\Delta M_a - \Delta M_b + 2\Delta B_2 M_2) - 3I_2^2 M_2$
			$+2(I_c - I_s)M_2$
E	1.2006(106)	$-\Delta B_2\Delta M_a - 2\Delta L_s M_2$	$+I_2(\Delta M_a + 2\Delta B_2 M_2) - 2I_2^2 M_2 - 2I_s M_2$
F	0.7479(95)	$-2\Delta L_c M_2$	$+2I_2\Delta M_a + 3I_2^2 M_2 - 2I_c M_2$
G	2.4698(52)	$-2\Delta L_l M_2 - 2\Delta L_c M_2$	$-2I_2\Delta M_a + 4I_2^2 M_2 - 2(I_l + I_c)M_2$
H	−2.2014(38)	$-2\Delta L_x M_2$	$-2I_x M_2$

TABLE IV. Group-by-group comparison of contributions to the electron anomaly calculated from the second and third columns of Tables I and III with the help of Table II. Infrared divergent terms are not included since they are common to both results.

Group	From Table I	From Table III	Difference
A	−0.7887(81)	−0.7921(52)	0.0034
B	−0.7779(78)	−0.7947(312)	0.0168
C	0.2793(85)	0.2823(99)	−0.0030
D	0.2126(174)	0.1990(201)	0.0136
E	0.6357(87)	0.6299(106)	0.0058
F	0.7509(160)	0.7486(97)	0.0023
G	2.3547(133)	2.3469(56)	0.0078
H	−1.7193(87)	−1.7218(45)	0.0025

(1.7) yields

$$a^{\text{th}} = (1\,159\,651.7_1 \pm 2.2_3)\times 10^{-9}\,, \qquad (1.9)$$

which is in fair agreement with the latest experimental value[19]

$$a^{\text{exp}} = (1\,159\,656.7 \pm 3.5)\times 10^{-9}\,. \qquad (1.10)$$

The uncertainty in (1.9) arises from two sources, one from the fine-structure constant (±2.2) and the other from theory (±0.33). The theoretical uncertainty is thus 6.7 times smaller than that of α in (1.8). Thus an improvement in the $g-2$ experiment will lead to a value of the fine-structure constant which is more accurate than the value (1.8), or ones determined by the fine-structure[20] and hyperfine-structure[21] measurements of hydrogen atom, the hyperfine splitting of the muonium ground state,[22] or the fine-structure measurement of the helium atom.[23]

The present theoretical uncertainty in the α^3 term of (1.7) will be eliminated before long by a complete analytic calculation of all sixth-order contributions. Then the theoretical value of the electron anomaly will be known to the accuracy of several $\times 10^{-11}$ since it has no bound-state complication and all conceivable effects such as the breakdown of quantum electrodynamics, hadronic corrections, and weak-interaction effects will be smaller than $(\alpha/\pi)^4$ in magnitude. Thus, further improvement in the experimental value of the electron anomaly will provide the cleanest and most accurate determination of the fine-structure constant. Particularly interesting will be the com-

TABLE V. In order to compare with the results of Levine and Wright (see Ref. 11) and Levine and Roskies (see Ref. 8), $\eta_i M_i$ of Table I are rewritten in the form $A+B(\ln\lambda)+C(\ln\lambda)^2$. The coefficients A, B, C are listed in columns 2, 5, 6, respectively. Also $\mu_1 = M_x = -0.4677$, $\mu_2 = \Delta M_l = 0.7775$, $\mu_3 = 2[\Delta M_c - (\frac{5}{4})M_2] = -0.5640$, $\mu_4 = 2[\Delta M_s + (\frac{1}{2})M_2] = -0.0900$.

Diagram	Present calculation	Levine *et al.*	Difference	Coefficients of $\ln\lambda$	Coefficients of $(\ln\lambda)^2$
$A1$	−2.4632(20)	−2.463 23	0.0000	$2\mu_4$	1
$A3$	−3.3685(62)	−3.374 31	0.0058	μ_4	$\frac{1}{2}$
$B3$	1.7873(50)	1.790 28	−0.0030		
$D2$	−3.9609(96)	−3.951(40)	−0.010	$2\mu_1$	
$D3$	6.5413(104)	6.541(13)	0.000	$\mu_3-\mu_4$	−1
$D5$	−0.0805(36)	−0.083(6)	0.003	$\mu_3-\mu_4$	−1
$E2$	−0.1465(72)	−0.153(6)	0.007	$2\mu_1$	
$F2$	5.4876(136)	5.515(25)	−0.027	$-2\mu_1$	
$F3$	−2.7326(58)	−2.746(7)	0.013	$-\mu_3$	$\frac{1}{2}$
$G2$	0.6096(34)	0.613(13)	−0.003	$-2\mu_1$	
$G3$	1.8572(86)	1.854(13)	0.003		
$G4$	−0.3182(72)	−0.330(13)	0.012		
$H2$	−1.7464(76)	−1.763(20)	0.017		
$H3$	−0.0307(27)	−0.021(100)	−0.010		
$A2+B2$	3.7986(56)	3.79838	0.0003	$4\mu_2$	
$-B2+D1$	2.3378(61)	2.342(13)	−0.004	$-2\mu_2+\mu_3-\mu_4$	−1
$A2+D1$	6.1364(73)	6.140(7)	−0.004	$2\mu_2+\mu_3-\mu_4$	−1
$A2+E1$	6.1042(60)	6.103(6)	0.001	$2\mu_2+\mu_3-\mu_4$	−1
$C2+D4$	−4.1928(87)	−4.206(25)	0.003	$-4\mu_2$	
$-C2+G5$	0.6291(67)	0.630(25)	−0.001	$2\mu_2-2\mu_3$	1
$C3+E3$	−3.1709(68)	−3.174(14)	0.003		
$D1-E1$	0.0322(64)	0.037(14)	−0.005		
$2\times E3+H1$	−1.2043(74)	−1.195(14)	−0.009	$-2\mu_1$	
$F1-G5$	−1.8210(82)	−1.836(13)	0.015		
$B1+2\times B2+G1$	−3.4206(80)	−3.418(20)	−0.003	$4\mu_2-\mu_3+3\mu_4$	2
$C1+2\times F1+H1$	0.0330(135)	0.036(26)	−0.003	$-2\mu_3-2\mu_4$	

parison of a's determined by the electron $g-2$ measurement and the ac Josephson effect.[24] We urge strongly that more accurate measurements of the electron $g-2$ value be undertaken as soon as possible.

II. PRELIMINARY REMARKS

Let $p-q/2$ and $p+q/2$ be the momenta of incoming and outgoing electron lines and $\tilde{\Gamma}^{\nu}(p,q)$ and $\Gamma^{\nu}(p,q)$ be the renormalized and unrenormalized proper vertex parts related to each other by[25]

$$\tilde{\Gamma}^{\nu}=(1-B)^{-1}\Gamma^{\nu}\ , \tag{2.1}$$

$(1-B)^{-1}\equiv Z_2$ being the wave-function renormalization constant. Then the anomalous magnetic moment of an electron $a=(g-2)/2$, i.e., the static limit of the magnetic form factor $F_2(q)$, is given by[26]

$$a=F_2(0)=\tilde{M}=(1-B)^{-1}M\ , \tag{2.2}$$

$$M=\lim_{q=0}\frac{1}{4p^4q^2}\,\mathrm{Tr}\left[\left(\gamma^{\nu}p^2-(1+q^2/2)\,p^{\nu}\right)(\not{p}+\not{q}/2+1)\times\Gamma_{\nu}(\not{p}-\not{q}/2+1)\right]\ .$$

(Throughout this paper we set electron mass $m_e=1$.) We also need the vertex renormalization constant L defined by

$$1+L=(1-B)\,F_1(0)=\tfrac{1}{4}\mathrm{Tr}\left[(1+\not{p})\,p^{\nu}\,\Gamma_{\nu}\right]_{q=0}\ . \tag{2.3}$$

Charge conservation requires that the charge form factor satisfy $F_1(0)=1$, or the Ward identity

$$B+L=0\ . \tag{2.4}$$

In perturbation theory a is expanded in a power series

$$a=\sum_{n=1}^{\infty}a^{(2n)}\left(\frac{\alpha}{\pi}\right)^n\ , \tag{2.5}$$

α being the fine-structure constant. Expanding B and M similarly in (2.2) we find[27]

$$\begin{aligned}a^{(2)}&=M^{(2)}\ ,\\ a^{(4)}&=M^{(4)}+B^{(2)}M^{(2)}\ ,\\ a^{(6)}&=M^{(6)}+B^{(2)}M^{(4)}+[B^{(4)}+(B^{(2)})^2]M^{(2)}\ ,\\ &\cdots .\end{aligned} \tag{2.6}$$

Let us examine the process of renormalization in more detail restricting ourselves to the group 4 diagrams, i.e., the three-photon exchange diagrams of Fig. 2. To each diagram we associate a contribution to the renormalized vertex part $\tilde{\Gamma}^{\nu}$ by Dyson's renormalization prescription. For example,

$$\tilde{\Gamma}^{\nu}_{E3}=\Gamma^{\nu}_{E3}-L_2\Gamma^{\nu}_{x}-(L_{E3}-L_2L_x)\,\gamma^{\nu}\ , \tag{2.7}$$

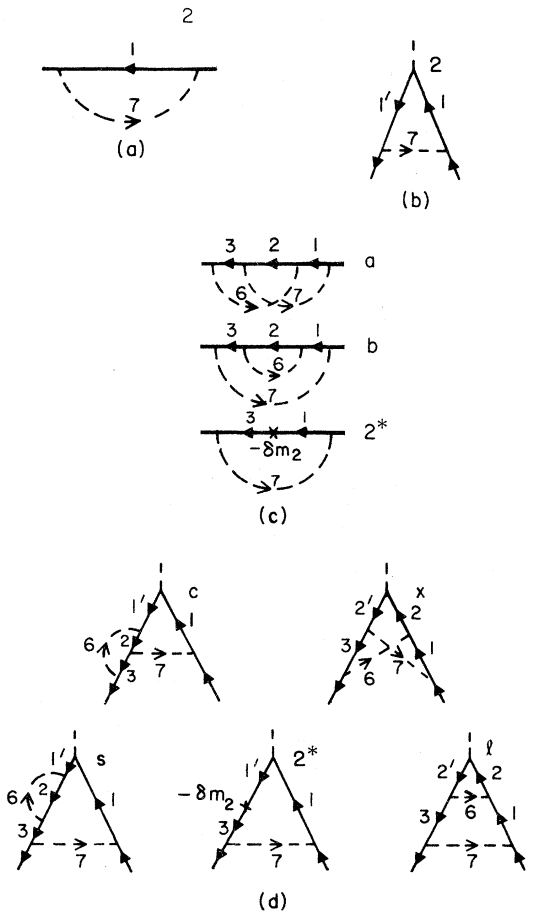

FIG. 4. (a) Second-order electron self-energy diagram. (b) Second-order vertex diagram. (c) Fourth-order electron self-energy diagrams a and b and the self-mass counterterm 2* for the diagram b. (d) Fourth-order vertex diagrams of the crossed ladder (x), corner (c), ladder (l), and self-energy-insertion (s) type, and the self-mass counterterm 2* for the diagram s.

where the subscripts refer to diagram designations of Fig. 2 and Figs. 4(b) and 4(d). L_2 is the vertex renormalization constant of second order, and L_x arises from the fourth-order crossed-ladder diagram. The overall renormalization factor L_{E3} is defined to satisfy

$$\tilde{\Gamma}^{\nu}_{E3}=0\ \text{ at }\ q=0\ . \tag{2.8}$$

The magnetic-moment projection of (2.7) yields

$$a_{E3}=M_{E3}-L_2M_x\ , \tag{2.9}$$

where M_{E3} and M_x are defined according to (2.2).

In general the anomaly term a_i may be written as

$$a_i=M_i+r_i\ , \tag{2.10}$$

where M_i is the contribution of diagram i in Fig. 2 and associated mass counterterms and r_i is the subtraction term. We list all r_i in Table VI. The

contribution of all diagrams of group 4 is given by

$$a_4^{(6)} = M^{(6)} - (5L^{(2)} + 4B^{(2)})M^{(4)} - (3L^{(4)} + 2B^{(4)})M^{(2)} + [5(B^{(2)})^2 + 16B^{(2)}L^{(2)} + 12(L^{(2)})^2]M^{(2)}. \quad (2.11)$$

$M^{(6)}$ is the contribution of all diagrams of Fig. 2 and mass counterterms. $M^{(4)}$, $L^{(4)}$ come from diagrams of Fig. 4(d). $B^{(4)}$ arises from the fourth-order self-energy diagrams of Fig. 4(c). The integer coefficients in (2.11) have a simple interpretation; they represent the number of ways insertions can be made. The Ward identity reduces (2.11) to (2.6).

We shall define Feynman integrals in terms of the parametric representation of I. Since relevant parametric functions are defined there, we shall freely quote them and their properties.

In the notation of I the $2n$th-order contributions to the vertex part and the electron self-energy part are expressed in the form

$$\left(\frac{\alpha}{\pi}\right)^n \Gamma_v^{(2n)} = \left(\frac{-\alpha}{4\pi}\right)^n (n-1)!\, \mathrm{F}_v \int \frac{dz}{U^2 V^n}, \quad (2.12)$$

$$\left(\frac{\alpha}{\pi}\right)^n \Sigma^{(2n)} = -\left(\frac{-\alpha}{4\pi}\right)^n (n-2)!\, \mathrm{F} \int \frac{dz}{U^2 V^{n-1}} \quad (2.13)$$

TABLE VI. Subtraction terms $a_i - M_i$ and $a_i - \Delta' M_i$ in the usual renormalization and K renormalization.

Diagram	$a_i - M_i$	$a_i - \Delta' M_i$
*A*1	$-2B_2(M_s - \delta m_2 M_2{}^*) + B_2{}^2 M_2$	$-2\Delta' B_2 \Delta M_s + (\Delta' B_2)^2 M_2$
*A*2	$-B_2 M_l - L_2(M_s - \delta m_2 M_2{}^*) + B_2 L_2 M_2$	$-\Delta' B_2 \Delta' M_l - \Delta' L_2 \Delta M_s + \Delta' B_2 \Delta' L_2 M_2$
*A*3	$-2B_2(M_s - \delta m_2 M_2{}^*) + B_2{}^2 M_2$	$-2\Delta' B_2 \Delta M_s + (\Delta' B_2)^2 M_2$
*B*1	$-B_2(M_s - \delta m_2 M_2{}^*) - (B_b - \delta m_2 B_2{}^*) M_2 - (\delta m_b - \delta m_2 \delta m_2{}^*) M_2{}^* + B_2{}^2 M_2$	$-\Delta' B_2 \Delta M_s - \Delta' \delta m_b M_2{}^* - \Delta' B_b M_2 + (\Delta' B_2)^2 M_2$
*B*2	$-B_2 M_l - (L_s - \delta m_2 L_2{}^*) M_2 + B_2 L_2 M_2$	$-\Delta' B_2 \Delta' M_l - \Delta' L_s M_2 + \Delta' B_2 \Delta' L_2 M_2$
*B*3	$-L_2 M_l - L_l M_2 + L_2{}^2 M_2$	$-\Delta' L_2 \Delta' M_l - \Delta' L_l M_2 + (\Delta' L_2)^2 M_2$
*C*1	$-2L_2(M_s - \delta m_2 M_2{}^*) - B_a M_2 + 2B_2 L_2 M_2 - \delta m_a M_2{}^*$	$-\Delta' \delta m_a M_2{}^* - 2\Delta' L_2 \Delta M_s - \Delta' B_a M_2 + 2\Delta' B_2 \Delta' L_2 M_2$
*C*2	$-L_2 M_l - L_c M_2 + L_2{}^2 M_2$	$-\Delta' L_2 \Delta' M_l - \Delta' L_c M_2 + (\Delta' L_2)^2 M_2$
*C*3	$-L_x M_2$	$-\Delta' L_x M_2$
*D*1	$-B_2 M_c - (L_s - \delta m_2 L_2{}^*) M_2 + B_2 L_2 M_2$	$-\Delta' B_2 \Delta M_c - \Delta' L_s M_2 + \Delta' B_2 \Delta' L_2 M_2$
*D*2	$-B_2 M_x$	$-\Delta' B_2 M_x$
*D*3	$-B_2 M_c - L_2(M_s - \delta m_2 M_2{}^*) + B_2 L_2 M_2$	$-\Delta' B_2 \Delta M_c - \Delta' L_2 \Delta M_s + \Delta' B_2 \Delta' L_2 M_2$
*D*4	$-L_2 M_c - L_2 M_l + L_2{}^2 M_2$	$-\Delta' L_2 \Delta M_c - \Delta' L_2 \Delta' M_l + (\Delta' L_2)^2 M_2$
*D*5	$-B_2 M_c - L_2(M_s - \delta m_2 M_2{}^*) + B_2 L_2 M_2$	$-\Delta' B_2 \Delta M_c - \Delta' L_2 \Delta M_s + \Delta' B_2 \Delta' L_2 M_2$
*E*1	$-B_2 M_c - (L_s - \delta m_2 L_2{}^*) M_2 + B_2 L_2 M_2$	$-\Delta' B_2 \Delta M_c - \Delta' L_s M_2 + \Delta' B_2 \Delta' L_2 M_2$
*E*2	$-B_2 M_x$	$-\Delta' B_2 M_x$
*E*3	$-L_2 M_x$	$-\Delta' L_2 M_x$
*F*1	$-L_2 M_c - L_c M_2 + L_2{}^2 M_2$	$-\Delta' L_2 \Delta M_c - \Delta' L_c M_2 + (\Delta' L_2)^2 M_2$
*F*2	$-L_2 M_x$	$-\Delta' L_2 M_x$
*F*3	$-2L_2 M_c + L_2{}^2 M_2$	$-2\Delta' L_2 \Delta M_c + (\Delta' L_2)^2 M_2$
*G*1	$-L_2 M_c - L_l M_2 + L_2{}^2 M_2$	$-\Delta' L_2 \Delta M_c - \Delta' L_l M_2 + (\Delta' L_2)^2 M_2$
*G*2	$-L_2 M_x$	$-\Delta' L_2 M_x$
*G*3	0	0
*G*4	0	0
*G*5	$-L_2 M_c - L_c M_2 + L_2{}^2 M_2$	$-\Delta' L_2 \Delta M_c - \Delta' L_c M_2 + (\Delta' L_2)^2 M_2$
*H*1	$-L_x M_2$	$-\Delta' L_x M_2$
*H*2	0	0
*H*3	0	0

where

$$dz = \delta(1 - \sum z_i) \prod dz_i, \quad z_i \geq 0 \text{ for all } i \ . \quad (2.14)$$

We also need an integral obtained by inserting a δm vertex in a vertex diagram of order $2n$

$$-\delta m \left(\frac{\alpha}{\pi}\right)^n \Gamma_\nu^{(2n)*} = \delta m \left(\frac{-\alpha}{4\pi}\right)^n n!\, \mathsf{F}_\nu^* \int \frac{dz}{U^2 V^{n+1}} \ . \quad (2.15)$$

Similar expressions for $\Sigma^{(2n)*}$, $\Gamma_\nu^{(2n)*}$, etc. can be written down using the rules of I. Explicit forms of U, V, F_ν, etc. are given in the following sections.

Renormalization constants $L^{(2n)}$ and $\delta m^{(2n)}$ are obtained from (2.12) and (2.13) by evaluating them for $q=0$, $\not{p}=1$. To obtain $B^{(2n)}$ we must evaluate $\partial\Sigma^{(2n)}/\partial p^\mu$. This leads to

$$\left(\frac{\alpha}{\pi}\right)^n B^{(2n)} = -\left(\frac{-\alpha}{4\pi}\right)^n (n-2)! \times \int \frac{dz}{U^2}\left[\mathsf{E}\,\frac{1}{V^{n-1}} + 2(n-1)\, G\mathsf{F}\,\frac{1}{V^n}\right], \quad (2.16)$$

where $2G = -p^\nu(\partial V/\partial p^\nu)$ evaluated at $q=0$, $p^2=1$, and

$$\mathsf{E} = \sum_i A_i \mathsf{F}_i \ , \quad (2.17)$$

F_i being derived from F by the replacement $(\not{D}_i + m_i) \to \not{p}$. A_i is the scalar current defined by (I.74), and the summation goes over electron lines only.

The renormalization program (2.10) can be carried out explicitly using these renormalization constants. From the computational point of view, however, this is not necessarily desirable since the subtraction terms r_i are generally infrared-divergent and make numerical evaluation of a_i difficult. In order to circumvent this problem systematically we have developed in II an alternative scheme which we briefly summarize here.[28]

Suppose the UV divergence of a diagram G arises from a subdiagram S consisting of N_S lines and n_S closed loops. Then the K_S operation on the Feynman integral $M_G \equiv \int dz\, J_G$ is defined by the following steps:

(a) Let all $z_i \in S$ be of order ϵ

$$\sum_{i\in S} z_i = \epsilon \to 0 \ .$$

(b) Keep only the lowest power of ϵ in all parametric functions B_{ij}, A_i, U, V, etc. In particular keep only the leading term of the integrand J_G.

(c) Replace the modified V by $V_S + V_{G/S}$, where V_S is the function V defined on the subdiagram S alone and $V_{G/S}$ is defined on the reduced diagram G/S obtained by shrinking S to a point.

(d) Rewrite J_G in terms of redefined parametric functions and call the result $K_S J_G$. The corresponding integral will be referred to as $K_S M_G$.

As is easily seen M_G is divergent in the limit $\epsilon \to 0$ if and only if

$$N_S - 2n_S - m_S \leq 0 \ , \quad (2.18)$$

where m_S is the maximum number of contractions of D_i operators within S. Throughout this paper we deal only with logarithmic divergences [equality in (2.18)]. Thus step (b) is sufficient to ensure that $(1-K_S)M_G$ is convergent for $\epsilon \to 0$. Since $V_{G/S} = O(1)$ and $V_S = O(\epsilon)$, step (c) does not affect the leading behavior in the $\epsilon \to 0$ limit. Though (c) is somewhat arbitrary, it enables us to avoid introducing an IR divergence in the subtraction terms. Furthermore it enables us to factor $K_S M_G$ into lower-order contributions as follows:

$$K_S M_G = \begin{cases} \hat{L}_S M_{G/S} & \text{if } S \text{ is a vertex subdiagram,} \\ \delta\hat{m}_S M_{T*} + \hat{B}_S M_T & \text{if } S \text{ is an electron self-energy subdiagram,} \end{cases} \quad (2.19)$$

where $\hat{L}_S$, $\delta\hat{m}_S$, $\hat{B}_S$ are the overall divergent parts of L_S, δm_S, B_S (see II for precise definitions), and T is obtained from $T^* \equiv G/S$ by shrinking one of the electron lines attached to the self-energy subdiagram to a point.

Let $\mathcal{S}$ be the set of all vertex and self-energy subdiagrams of G. Then the integral

$$\Delta' M_G = \prod_{S_i \in \mathcal{S}} (1 - K_{S_i}) M_G \quad (2.20)$$

is UV-divergence-free by construction. This is a kind of intermediate renormalization and $\Delta' M_G$ will be referred to as K-renormalized or K-finite. In II we have shown that the quantity $\bar{M}_G$ renormalized in the usual way can be expressed in terms of K-renormalized quantities as

$$\bar{M}_G = \prod_{S\in\mathcal{S}} (1 - \Delta' \mathcal{C}_S)\, \Delta' M_G \ , \quad (2.21)$$

where $\Delta' \mathcal{C}_S$ is an operator extracting the K-finite part of the renormalization constant associated with the subdiagram S.

Infrared divergences, which are generally present in $\Delta' M_G$, can be handled in a similar way in terms of $I_{G/S}$ operation defined as follows:

(a′) Set

$$z_i = \begin{cases} O(\delta) \text{ if } i \text{ is an electron line in } G/S, \\ O(1) \text{ if } i \text{ is a photon line in } G/S \ , \\ O(\epsilon)\ \epsilon \simeq \delta^2, \text{ if } i \in S \ . \end{cases}$$

(b′) Keep only the lowest powers of ϵ, δ in all parametric functions.

(c′) Modify the results of (b′) as follows:

$$U \to U_S U_{G/S},\quad V \to V_S + V_{G/S},\quad \mathsf{F} \to F_0[L_{G/S}]\,\mathsf{F}_S\,,$$

where $F_0[L_{G/S}]$ is the no-contraction term of the vertex renormalization constant defined on G/S, and F_S is the product of γ matrices and D_i^μ operators for the diagram S alone.

(d′) Rewrite the integrand J_G in terms of redefined parametric functions and call the result as $I_{G/S}J_G$. The corresponding integral will be denoted as $I_{G/S}M_G$.

Step (a′) is a twofold limit; $\epsilon \to 0$ by itself is just the UV limit for subdiagram S, and $\delta \to 0$ corresponds to all photons of the reduced diagram G/S going to the IR limit. Step (c′) is arbitrary and is chosen to insure a desirable factorization of the subtraction term. All modifications in (c′) are order δ smaller than the leading terms so that they affect the integrand only away from the divergent region. By choosing the redefinitions (c′), we can avoid detailed study of the IR structure of the diagram G/S; in actual calculation we will be able to cancel such terms among themselves without computing them explicitly.

Let S_i be the set of all subdiagrams such that G/S_i are IR-divergent. Then the integral

$$\Delta M_G = \prod_i (1 - I_{G/S_i})\,\Delta' M_G \tag{2.22}$$

is free from both UV and IR divergences by construction. It is ΔM_G that we evaluate on the computer.

The above procedures split Feynman integrals into a number of pieces with different UV and IR properties. We will use the following notation to distinguish between these:

Let M_i be a Feynman integral with (logarithmic) UV and IR divergences. Then, $\hat{M}_i$, the overall UV-divergent part of M_i, is the portion of M_i for which the integrand cannot be defined without regularization; $\Delta' M_i$, the K-finite part of M_i, is obtained by projecting out the UV divergences by the K_S operation; I_i, the overall IR-divergent part of M_i, arises from the portion of M_i which diverges when all photons in diagram i are soft; ΔM_i is the UV- and IR-finite portion of M_i where all divergences have been projected out by K_S and $I_{G/S}$ operations.

Techniques of I and II have been developed primarily for higher-order calculations. However, since we need renormalization constants of second and fourth orders to renormalize sixth-order terms, we shall first illustrate our method by applying it to the second- and fourth-order integrals.

III. RENORMALIZATION CONSTANTS OF SECOND ORDER

According to (2.12) the second-order vertex part is given by

$$\Gamma_2^\nu = -\tfrac{1}{4}\,\mathsf{F}^\nu \int \frac{dz}{U^2 V}\quad , \tag{3.1}$$

where

$$\begin{aligned} &\mathsf{F}^\nu = \gamma^\mu (\not{p}_{1'} + m_{1'})\,\gamma^\nu (\not{p}_1 + m_1)\,\gamma_\mu\ , \\ &D_i^\mu = \tfrac{1}{2}\int_{m_i^2}^{\infty} dm_i^{\,2}\,\frac{\partial}{\partial q_{i\mu}}\ ,\quad i = 1, 1' \end{aligned} \tag{3.2}$$

in the notation of Fig. 4(b). Introducing the Feynman cutoff Λ for the photon 7 and carrying out the D operations, we can reduce (3.1) to

$$\Gamma_2^\nu = -\tfrac{1}{4}\int dz \int_{\lambda^2}^{\Lambda^2} z_7\, dm_7^{\,2}\left(\frac{F_0^\nu}{U^2V^2} + \frac{F_1^\nu}{U^3 V}\right), \tag{3.3}$$

where λ is the infinitesimal photon mass and

$$\begin{aligned} &F_0^\nu = \gamma^\mu (\not{Q}_1' + m_{1'})\,\gamma^\nu (\not{Q}_1' + m_1)\,\gamma_\mu\ , \\ &F_1^\nu = -\tfrac{1}{2} B_{11'}\,\gamma^\mu \gamma^\lambda \gamma^\nu \gamma_\lambda \gamma_\mu\ . \end{aligned} \tag{3.4}$$

(Q_i' and B_{ij} are defined below.) We emphasize that λ^2 and Λ^2 are introduced only to facilitate our argument: The integrals we will actually evaluate will have no Λ^2 dependence; the photon mass will be set equal to zero. The vertex renormalization constant L_2 is obtained by evaluating (3.3) for $q = 0$, $\not{p} = 1$. For $q = 0$ we have $\not{Q}_i' = A_i \not{p}$ by (I.78), A_i being the scalar current. Noting that $A_1 = A_{1'}$, $B_{11} = B_{11'} = B_{1'1'}$ by (I.40) and (I.44), and applying the projection (2.3), we find

$$L_2 = -\tfrac{1}{4}\int dz \int_{\lambda^2}^{\Lambda^2} z_7\, dm_7^{\,2}\left(\frac{F_0}{U^2V^2} + \frac{F_1}{U^3 V}\right), \tag{3.5}$$

with

$$\begin{aligned} &F_0 = -2(1 - 4A_1 + A_1^{\,2})\ , \\ &F_1 = -2B_{11}\ . \end{aligned} \tag{3.6}$$

We must now find the parametric functions A_1, B_{11}, U, and V necessary to define the integral (3.5). From (I.54) and (I.1) we obtain

$$\begin{aligned} &B_{11} = 1\ , \\ &U = z_1 + z_{1'} + z_7 = z_{11'7}\ . \end{aligned} \tag{3.7}$$

By choosing $q_7 = -p$, $q_1 = q_{1'} = 0$, we obtain from (I.2)

$$A_1 = z_7 B_{11}/U = z_7/z_{11'7}\quad . \tag{3.8}$$

To define V it is most convenient to choose $q_1 = q_{1'} = p$, $q_7 = 0$ in (I.3) and (I.36):

$$\begin{aligned} &V = z_{11'} + m_7^{\,2} z_7 - G\ , \\ &G = z_{11'} A_1\ \ (p^2 = 1)\ . \end{aligned} \tag{3.9}$$

Finally we need

$$dz = \delta(1 - z_{11'7})\, dz_1\, dz_{1'}\, dz_7 \ . \tag{3.10}$$

One can of course obtain (3.5) directly without going through the steps outlined here. Note, however, that the general procedure of setting up a parametric integral for any diagram is no more complicated than the one shown above.

Since z_1 and $z_{1'}$ appear in the combined form $z_{11'}$ in (3.5), we can perform one integration over z and reduce (3.5) to

$$L_2 = -\tfrac{1}{4}\int dz \int_{\lambda^2}^{\Lambda^2} z_{11'} z_7\, dm_7^2 \left(\frac{F_0}{U^2V^2} + \frac{F_1}{U^3V}\right), \tag{3.11}$$

using the new definition of dz

$$dz = \delta(1 - z_{11'} - z_7)\, dz_{11'}\, dz_7 \ . \tag{3.12}$$

As is easily checked, only the F_1 term satisfies the divergence criterion (2.18). We shall therefore define the UV-divergent part $\hat{L}_2$ of L_2 [see (2.19)] by

$$\hat{L}_2 = -\tfrac{1}{4}\int dz \int_{\lambda^2}^{\Lambda^2} z_7\, dm_7^2\, \frac{z_{11'} F_1}{U^3 V} = \tfrac{1}{2}(\ln\Lambda - \tfrac{1}{4}) \ . \tag{3.13}$$

Since the remainder is UV-finite, we can perform the m_7 integration and obtain

$$L_2 - \hat{L}_2 = \Delta' L_2 = -\tfrac{1}{4}\int dz\, \frac{z_{11'} F_0}{U^2 V} \ . \tag{3.14}$$

Carrying out the z integration we find

$$\Delta' L_2 = \ln\lambda + \tfrac{5}{4} \equiv I_2 \ , \tag{3.15}$$

where I_2 is introduced to emphasize that (3.15) is IR-divergent. From (3.13) and (3.15) we obtain the standard result

$$L_2 = \hat{L}_2 + I_2 = \tfrac{1}{2}\ln\Lambda + \ln\lambda + \tfrac{9}{8} \ . \tag{3.16}$$

In the second order only one diagram [Fig. 4(a)] contributes to the electron mass operator [see (2.13)]

$$\Sigma_2(p) = \tfrac{1}{4}\,\mathsf{F}\int dz \int z_7\, dm_7^2\, \frac{1}{U^2 V} \ , \qquad \mathsf{F} = \gamma^\mu(\not{D}_1 + m_1)\gamma_\mu \ . \tag{3.17}$$

Carrying out the F operation and setting $\not{p} = 1$, we get

$$\delta m_2 = \tfrac{1}{4}\int dz \int z_7\, dm_7^2\, \frac{F_0}{U^2 V}, \qquad F_0 = 2(2 - A_1) \ . \tag{3.18}$$

Note that this F_0 is different from that of (3.6). Integration of (3.18) can be easily performed, yielding the IR-divergence-free result

$$\delta m_2 = \tfrac{3}{2}(\ln\Lambda + \tfrac{1}{4}) \ . \tag{3.19}$$

According to (2.16) the wave-function renormalization constant is given by

$$B_2 = \tfrac{1}{4}\int dz \int z_7\, dm_7^2 \left(\mathsf{E}\,\frac{1}{U^2 V} + 2G\,\mathsf{F}\,\frac{1}{U^2 V^2}\right), \tag{3.20}$$

where G is defined by (3.9) with $z_1 \to z_{11'}$ and $\mathsf{E} = [\gamma^\mu(A_1\not{p})\gamma_\mu]_{\not{p}=1}$. This reduces to

$$B_2 = \tfrac{1}{4}\int dz \int z_7\, dm_7^2 \left(\frac{E_0}{U^2 V} + \frac{2GF_0}{U^2 V^2}\right), \tag{3.21}$$

where F_0 is given by (3.18) and $E_0 = -2A_1$.

Note that, if we identify z_1 in (3.21) and $z_{11'}$ in (3.5), all parametric functions defining B_2 and L_2 become identical. In general parametric functions independent of the external photon momentum q are common for a self-energy diagram and the corresponding set of vertex diagrams.

The UV-divergent part of B_2 [see (2.19)] is

$$\hat{B}_2 = \tfrac{1}{4}\int dz \int z_7\, dm_7^2\, \frac{E_0}{U^2 V} = -\tfrac{1}{2}(\ln\Lambda + \tfrac{5}{4}) \ , \tag{3.22}$$

while the remainder

$$\Delta' B_2 = \tfrac{1}{4}\int dz\, \frac{2GF_0}{U^2 V} \tag{3.23}$$

is still IR-divergent. To separate the IR-divergent part, let us rewrite the integrand of $\Delta' B_2$ as

$$2GF_0 = -2z_1(1 - 4A_1 + A_1^2) + 2z_1(1 - A_1^2) \ . \tag{3.24}$$

The first term is identical with the integrand F_0 of (3.14). The second term vanishes for $A_1 \to 1$ and hence is IR-finite. Thus we can write

$$\Delta' B_2 = -I_2 + \Delta B_2 \ , \tag{3.25}$$

where

$$\Delta B_2 = \tfrac{1}{4}\int dz\, \frac{2z_1(1 - A_1^2)}{U^2 V} = \tfrac{3}{4} \ . \tag{3.26}$$

Collecting all parts of B_2 we find

$$B_2 = -L_2 \tag{3.27}$$

in agreement with the Ward identity (2.4).

IV. RENORMALIZATION CONSTANTS OF FOURTH ORDER

Two diagrams contribute to the mass operator $\Sigma^{(4)}(p)$. Let us first discuss the contribution of diagram a in Fig. 4(c)

$$\Sigma_a(p) = -\tfrac{1}{16}\,\mathsf{F}\int dz \int_{\lambda^2}^{\Lambda^2} z_6\, dm_6^2 \int_{\lambda^2}^{\Lambda^2} z_7\, dm_7^2\, \frac{2}{U^2 V^3} \ . \tag{4.1}$$

The self-mass is obtained by carrying out the F operation and setting $\not{p} = 1$ in (4.1):

$$\delta m_a = -\tfrac{1}{16}\int dz \int z_6\, dm_6^2 \int z_7\, dm_7^2 \left(\frac{2F_0}{U^2 V^3} + \frac{F_1}{U^3 V^2}\right), \tag{4.2}$$

where

$$F_0 = 4(-2 + A_1 + A_2 + A_3 + A_1A_2 + A_1A_3 + A_2A_3 - 2A_1A_2A_3) , \quad (4.3)$$
$$F_1 = 4[B_{12}(A_3 - 2) + B_{13}(4A_2 - 2) + B_{23}(A_1 - 2)] .$$

Applying the rules of I we find

$$B_{12} = z_{36}, \quad B_{13} = -z_2, \quad B_{23} = z_{17} ,$$
$$U = z_2(z_{17} + z_{36}) + z_{17}z_{36} ,$$
$$A_i = 1 - (z_1B_{1i} + z_2B_{2i} + z_3B_{3i})/U, \quad i = 1, 2, 3 \quad (4.4)$$
$$G = z_1A_1 + z_2A_2 + z_3A_3 ,$$
$$V = z_{123} + m_6^2 z_6 + m_7^2 z_7 - G ,$$
$$dz = \delta(1 - z_{12367})\, dz_1\, dz_2\, dz_3\, dz_6\, dz_7 .$$

The F_1 term of (4.2) is UV-divergent since it satisfies (2.18) with $N_S = 5$, $n_S = 2$, $m_S = 1$. The F_0 term is free from both overall and subdiagram (e.g., $\{1, 2, 7\}$) UV divergences. Let us denote these two parts [see (2.19)] as

$$\delta\hat{m}_a = -\tfrac{1}{16}\int dz \int z_6\, dm_6^2 \int z_7\, dm_7^2\, \frac{F_1}{U^3V^2} , \quad (4.5)$$

$$\Delta'\delta m_a = -\tfrac{1}{16}\int dz\, \frac{F_0}{U^2V} . \quad (4.6)$$

According to (2.16) the wave-function renormalization constant from diagram a can be written as

$$B_a = -\tfrac{1}{16}\int dz \int z_6\, dm_6^2 \int z_7\, dm_7^2 \left[\frac{2E_0}{U^2V^3} + \frac{E_1}{U^3V^2} + 4G\left(\frac{3F_0}{U^2V^4} + \frac{F_1}{U^3V^3}\right)\right] , \quad (4.7)$$

where F_0, F_1 are given by (4.3) and

$$E_0 = 4[A_1 + A_2 + A_3 + 2(A_1A_2 + A_1A_3 + A_2A_3) - 6A_1A_2A_3] , \quad (4.8)$$
$$E_1 = 4(B_{12}A_3 + 4B_{13}A_2 + B_{23}A_1) .$$

The E_1 term satisfies the divergence criterion (2.18) for the whole diagram. Let us denote this overall divergent contribution as

$$\hat{B}_a = -\tfrac{1}{16}\int dz \int z_6\, dm_6^2 \int z_7\, dm_7^2\, \frac{E_1}{U^3V^2} . \quad (4.9)$$

The difference $B_a - \hat{B}_a$ is still UV-divergent because of divergent subvertices S (lines 1, 2, 7 and 2, 3, 6). For instance, the limit $z_{236} = \epsilon \to 0$, the F_1 term satisfies (2.18) with $N_S = 3$, $n_S = 1$, $m_S = 1$. The F_1 term is also divergent for $z_{127} \to 0$. The remaining terms of B_a are UV-finite.

To separate out these divergences systematically we have introduced the K_S operation described in Sec. II. Applied to the 236 vertex, step (b) of the K_S operation gives

$$B_{12} \to 0, \quad B_{13} \to 0, \quad B_{23} \to z_{17} ,$$
$$U \to U_S\, U_{G/S} \quad (U_S = z_{236}, \quad U_{G/S} = z_{17}) ,$$
$$A_1 \to A_1^{G/S} \equiv 1 - z_1/z_{17} , \quad (4.10)$$
$$G \to G^{G/S} = z_1A_1^{G/S} ,$$
$$V \to V^{G/S} = z_1 + m_7^2 z_7 - G^{G/S} .$$

$A_2^{G/S}$ and $A_3^{G/S}$ appear multiplied by B_{13}, B_{12} (in F_1) or z_2, z_3 (in V) and hence can be ignored. Step (c) leads to

$$V \to V_S + V_{G/S}, \quad V_S = z_{23}(1 - A_2^S) + m_6^2 z_6 , \quad (4.11)$$
$$A_2^S = 1 - z_{23}/z_{236} .$$

Thus we obtain (setting $T = G/S$)

$$K_S\left[\frac{2GF_1}{U^3V^3}\right] = \frac{F_1[L_S]}{U_S^3}\ \frac{2G_T\, F_0[B_T]}{U_T^2}\ \frac{1}{(V_S + V_T)^3} , \quad (4.12)$$

with

$$F_1[L_S] = -2B_{23}^S \quad (B_{23}^S = 1) ,$$
$$F_0[B_T] = -2(A_1^T - 2) , \quad (4.13)$$

where $F_1[L_S]$ is related to the UV-divergent part of L_2 in (3.5) for the vertex $S = \{2, 3, 6\}$ and $F_0[B_T]$ corresponds to the finite portion of B_2 in (3.21) for the reduced diagram $T = \{1, 7\}$. The notation we have introduced in (4.12), though excessive for such a simple result, is of the form applicable to any divergent subvertex.

The subvertex $S' = \{1, 2, 7\}$ leads to similar UV divergence. We can therefore define the UV-finite portion of B_a by

$$\Delta' B_a = -\tfrac{1}{16}\int dz \left[\frac{E_0}{U^2V} + \frac{2GF_0}{U^2V^2} + (1 - K_S - K_{S'})\,\frac{2GF_1}{U^3V}\right] . \quad (4.14)$$

Next we shall show that the integral of (4.12), i.e.,

$$K_S(B_a - \hat{B}_a) = -\tfrac{1}{16}\int dz \int z_6\, dm_6^2 \int z_7\, dm_7^2 K_S\left[\frac{4GF_1}{U^3V^3}\right] , \quad (4.15)$$

factorizes as in (2.19). For this purpose let us scale z_i as

$$z_m \to s z_m, \quad \text{for } m \in S$$
$$z_i \to t z_i , \quad \text{for } i \in T \quad (4.16)$$

where the new z's satisfy

$$\sum_{m \in S} z_m = 1, \quad \sum_{i \in T} z_i = 1 . \quad (4.17)$$

Then (4.15) becomes

$$-\tfrac{1}{16}\int dz_S \int z_6\, dm_6^{\,2}\, \frac{F_1[L_S]}{U_S^{\,3}} \int dz_T \int z_7\, dm_7^{\,2}\, \frac{2G_T F_0[B_T]}{U_T^{\,2}} \int \frac{2\delta(1-s-t)\, ds\, t\, dt}{(s V_S + t V_T)^3}\,, \tag{4.18}$$

where

$$\begin{aligned} dz_S &= \delta(1-z_{236})\, dz_2\, dz_3\, dz_6\,, \\ dz_T &= \delta(1-z_{17})\, dz_1\, dz_7\,. \end{aligned} \tag{4.19}$$

The integral over s and t in (4.18) is equal to $V_S^{-1} V_T^{-2}$ as is easily seen using the Feynman formula (I.19). Thus (4.18) factorizes as

$$\left[-\tfrac{1}{4}\int dz_S \int z_6\, dm_6^{\,2}\, \frac{F_1[L_S]}{U_S^{\,3} V_S}\right]\left[\tfrac{1}{4}\int dz_T\, \frac{2G_T F_0[B_T]}{U_T^{\,2} V_T}\right]. \tag{4.20}$$

Note that the photon 7 no longer needs regularization. Recalling the definitions (3.5) and (3.23), we may cast the result of this calculation in the form

$$K_S(B_a - \hat{B}_a) = \hat{L}_2 \Delta' B_2\,. \tag{4.21}$$

Similarly we have

$$K_{S'}(B_a - \hat{B}_a) = \hat{L}_2 \Delta' B_2\,. \tag{4.22}$$

These are examples of the general result (2.19). The above result may be summarized as follows:

$$B_a = \hat{B}_a + 2\hat{L}_2 \Delta' B_2 + \Delta' B_a\,. \tag{4.23}$$

The term $\Delta' B_a$ defined by (4.14) is UV-finite. But it still is divergent in the (overall) IR limit where the momenta of *both* internal photons vanish. In the Feynman parametric space this limit corresponds to

$$z_6 + z_7 = 1 - \delta, \quad \delta \to 0\,. \tag{4.24}$$

By studying the behavior of the integrand in this limit, it is easily seen that only the F_0 term of (4.14) gives rise to an IR-divergent integral

$$I_a = -\tfrac{1}{16}\int dz\, \frac{2GF_0}{U^2 V^2}\,. \tag{4.25}$$

We shall postpone the consideration of this integral until we define the overall IR divergences of the associated vertex diagrams.

These vertex diagrams are generated by inserting an external vertex in the electron lines of diagram a. Let us first consider the vertex renormalization constant for the crossed diagram in Fig. 4(d):

$$L_x = \tfrac{1}{16}\int dz \int z_6\, dm_6^{\,2} \int z_7\, dm_7^{\,2} \left(\frac{6F_0}{U^2 V^4} + \frac{2F_1}{U^3 V^3} + \frac{F_2}{U^4 V^2}\right), \tag{4.26}$$

where

$$\begin{aligned} F_0 &= 4[(1+A_2^{\,2})(1+A_1+A_3-2A_1A_3) \\ &\quad +2A_2(-2+A_1+A_3+A_1A_3)]\,, \\ F_1 &= -4[B_{12}(1+4A_2+A_3-2A_2A_3) \\ &\quad +B_{22}(-1-A_1-A_3+2A_1A_3) \\ &\quad +B_{23}(1+A_1+4A_2-2A_1A_2) \\ &\quad +4B_{13}(-1+A_2-A_2^{\,2})]\,, \\ F_2 &= 8(B_{12}B_{23}+2B_{12}B_{13}+2B_{13}B_{23})\,. \end{aligned} \tag{4.27}$$

The UV divergence is confined to the F_2 term. Hence

$$\hat{L}_x = \tfrac{1}{16}\int dz \int z_6\, dm_6^{\,2} \int z_7\, dm_7^{\,2}\, \frac{F_2}{U^4 V^2}\,. \tag{4.28}$$

Since there is no divergent subdiagram, the rest is UV-finite. But it is still IR-divergent and can be divided into the overall IR-divergent term I_x and the finite term ΔL_x:

$$\begin{aligned} I_x &= \tfrac{1}{16}\int dz\, \frac{F_0}{U^2 V^2}\,, \\ \Delta L_x &= \tfrac{1}{16}\int dz\, \frac{F_1}{U^3 V}\,. \end{aligned} \tag{4.29}$$

Thus we have

$$L_x = \hat{L}_x + I_x + \Delta L_x\,. \tag{4.30}$$

For the corner diagram in Fig. 4(d), the integrals for L_c, $\hat{L}_c$, I_c, etc. are given by (4.26), (4.28), (4.29) again except that F_0, F_1, F_2 are now

$$\begin{aligned} F_0 &= 4[1-4A_1+A_1^{\,2}+(A_2+A_3)(1+A_1)^2 \\ &\quad -2A_2A_3(1-A_1+A_1^{\,2})]\,, \\ F_1 &= 4[B_{11}(1+A_2+A_3-2A_2A_3) \\ &\quad +B_{12}(-1-4A_1-A_3+2A_1A_3) \\ &\quad +B_{13}(-1-4A_1-A_2+8A_1A_2) \\ &\quad +B_{23}(1-4A_1+A_1^{\,2})]\,, \\ F_2 &= 4(B_{11}B_{23}-4B_{12}B_{13})\,. \end{aligned} \tag{4.31}$$

However, the difference $L_c - \hat{L}_c$ is now UV-divergent due to the subdiagram $S = \{2, 3, 6\}$. By the same analysis that led to (4.14) we find the UV-finite part of L_c to be

$$\Delta' L_c = \tfrac{1}{16}\int dz \left[\frac{F_0}{U^2 V^2} + (1-K_S)\frac{F_1}{U^3 V}\right]. \tag{4.32}$$

This can be split further into the IR-divergent and IR-finite parts:

$$I_c = \tfrac{1}{16}\int dz\,\frac{F_0}{U^2V^2}\,,$$
$$\Delta L_c = \tfrac{1}{16}\int dz(1-K_S)\frac{F_1}{U^3V}\,. \tag{4.33}$$

Thus L_c can be written in the form

$$L_c = \hat{L}_c + \hat{L}_2\Delta' L_2 + I_c + \Delta L_c\,. \tag{4.34}$$

B_a, L_x, and L_c satisfy the Ward identity

$$B_a + L_x + 2L_c = 0\,. \tag{4.35}$$

This means in particular that the sum $I_a + I_x + 2I_c$ is free from the IR divergence. In order to evaluate this sum, it is useful to note that, if we replace $z_{22'}$ by z_2 in all parametric functions of the crossed diagram, they reduce to the corresponding functions of the self-energy diagram of Fig. 4(c). For this reason we have not distinguished the parametric functions in (4.1) and (4.26). Similar comment applies to the corner diagram in Fig. 4(d). The only difference among these diagrams is in the phase space, which can be written as

$$dz_{c_1} = z_1\,dz_a\,,$$
$$dz_x = z_2\,dz_a\,, \tag{4.36}$$
$$dz_{c_3} = z_3\,dz_a\,,$$

where the suffixes a, c_1, x, c_3 refer to the respective diagrams. Thus we find

$$I_x + 2I_c = \tfrac{1}{16}\int dz_a\,\frac{z_1F_0^{(1)} + z_2F_0^{(2)} + z_3F_0^{(3)}}{U^2V^2}\,, \tag{4.37}$$

where $F_0^{(1)}$, $F_0^{(2)}$, $F_0^{(3)}$ correspond to c_1, x, c_3, respectively.

This integral is very similar in form to I_a of (4.25). In fact, using the identity (for $p^2 = 1$)

$$2A_i(A_i\not{p} + 1) = (A_i\not{p} + 1)\not{p}(A_i\not{p} + 1) - (1-A_i^2)\not{p}\,, \qquad i = 1,2,3 \tag{4.38}$$

we can rewrite the numerator $2GF_0^{(a)}$ of (4.25) as

$$2GF_0^{(a)} = \sum_{i=1}^{3} z_i F_0^{(i)} + H\,, \tag{4.39}$$

where

$$H = -\sum_{i=1}^{3} z_i(1-A_i^2)H^{(i)}\,. \tag{4.40}$$

By simple manipulation we find

$$H^{(1)} = 4(1 + A_2 + A_3 - 2A_2A_3)\,,$$
$$H^{(2)} = 4(1 + A_1 + A_3 - 2A_1A_3)\,, \tag{4.41}$$
$$H^{(3)} = 4(1 + A_1 + A_2 - 2A_1A_2)\,.$$

From (4.25), (4.37), and (4.39) we obtain

$$I_a + I_x + 2I_c = -\tfrac{1}{16}\int dz_a\,\frac{H}{U^2V^2}\,. \tag{4.42}$$

Since $H \to 0$ as $A_i \to 1$ [see (4.40)], this is IR-finite as expected.

Let us define the UV- and IR-finite part of B_a by

$$\Delta B_a = -\tfrac{1}{16}\int dz\left[\frac{E_0}{U^2V} + \frac{H}{U^2V^2} + (1-K_S-K_{S'})\frac{2GF_1}{U^3V}\right]. \tag{4.43}$$

Then we can write $\Delta' B_a$ of (4.14) as

$$\Delta' B_a = \Delta B_a - I_x - 2I_c\,. \tag{4.44}$$

We shall now consider the self-energy diagram b of Fig. 4(c). $\Sigma_b(p)$, δm_b, and B_b are of the same form as (4.1), (4.2), and (4.7) where, however,

$$F_0 = 4[4(1-A_1+A_1^2) + A_2(1-4A_1+A_1^2)]\,,$$
$$F_1 = -4[3B_{12}A_1 + 8(B_{11}-B_{12})]\,,$$
$$E_0 = 4[4(-A_1+2A_1^2) + A_2(1-8A_1+3A_1^2)]\,, \tag{4.45}$$
$$E_1 = -12B_{12}A_1\,.$$

The parametric functions are

$$B_{11} = z_{26}\,,\quad B_{12} = z_6\,,$$
$$U = z_{137}z_{26} + z_2z_6\,,$$
$$A_i = z_7B_{1i}/U\,,\quad i \neq 7 \tag{4.46}$$
$$G = z_7(1-A_1)\,,$$
$$dz = \delta(1-z_{12367})\,z_{13}\,dz_{13}\,dz_2\,dz_6\,dz_7\,.$$

The overall UV-divergent part $\delta\hat{m}_b$ of δm_b can be defined as in (4.5). However, the difference

$$\delta m_b - \delta\hat{m}_b = -\tfrac{1}{16}\int dz\int z_6\,dm_6^2\,\frac{F_0}{U^2V^2} \tag{4.47}$$

still contains a UV divergence arising from the $z_{26} \to 0$ (self-energy subdiagram) region. We must therefore apply the K_S operation to extract the divergent part, where $S = \{2,6\}$. This leads to the UV-finite part

$$\Delta'\delta m_b = -\tfrac{1}{16}\int dz(1-K_S)\frac{F_0}{U^2V}\,. \tag{4.48}$$

Following the method in II we find that $K_S\delta m_b$ factorizes as

$$K_S\delta m_b = \hat{B}_2\delta m_2 + \delta m_2\delta m_{2*}\,, \tag{4.49}$$

where δm_{2*} is the self-energy contribution of the diagram 2* of Fig. 4(c). By a similar calculation we obtain

$$K_S\delta\hat{m}_b = \hat{B}_2\delta m_2 + \delta m_2\delta\hat{m}_{2*}\,, \tag{4.50}$$

where $\delta\hat{m}_{2*}$ is the UV-divergent part of δm_{2*}. [These are special cases of (2.19).] Thus we find

$$\delta m_b = \delta\hat{m}_b + \delta m_2\Delta\delta m_{2*} + \Delta'\delta m_b\,, \tag{4.51}$$

where $\Delta\delta m_{2*}$ is the UV-finite part of δm_{2*} and $\Delta'\delta m_b$ is given by (4.48).

Next let us examine B_b. As is easily seen $B_b - \hat{B}_b$, where $\hat{B}_b$ is of the form (4.9), contains a UV divergence arising from $S=\{2,6\}$. The UV-finite part of $B_b - \hat{B}_b$ is given by

$$\Delta' B_b = -\tfrac{1}{16}\int dz(1-K_S)\left(\frac{E_0}{U^2V}+\frac{2GF_0}{U^2V^2}+\frac{2GF_1}{U^3V}\right). \tag{4.52}$$

Splitting this into the overall IR-divergent part

$$I_b = -\tfrac{1}{16}\int dz(1-K_S)\frac{2GF_0}{U^2V^2} \tag{4.53}$$

and the completely finite remainder ΔB_b, we can write

$$B_b = \hat{B}_b + \delta m_2 \Delta' B_{2*} + \hat{B}_2 \Delta' B_2 + I_b + \Delta B_b , \tag{4.54}$$

where $\Delta' B_{2*}$ is defined by the diagram 2* of Fig. 4(c).

The vertex diagrams associated with the self-energy diagram b are shown in Fig. 4(d). The vertex renormalization constant L_s from the self-energy insertion diagram is of the form (4.26) with redefined F_0, F_1, F_2:

$$\begin{aligned} F_0 &= 4[(4A_1-2A_2)(1-A_1+A_1^2) \\ &\quad +(-2+A_1A_2)(1-4A_1+A_1^2)] , \\ F_1 &= 12[B_{11}A_1(-4+A_2) \\ &\quad +B_{12}(-1+6A_1-2A_1^2)] , \\ F_2 &= -12B_{11}B_{12} . \end{aligned} \tag{4.55}$$

Analogous to (4.54) we can split L_s as

$$L_s = \hat{L}_s + \delta m_2 \Delta' L_{2*} + \hat{B}_2 \Delta' L_2 + I_s + \Delta L_s , \tag{4.56}$$

where $\hat{L}_s$ is the UV-divergent term similar to (4.28),

$$I_s = \tfrac{1}{16}\int dz(1-K_S)\frac{F_0}{U^2V^2} \tag{4.57}$$

is the overall IR-divergent term, and

$$\Delta L_s = \tfrac{1}{16}\int dz(1-K_S)\frac{F_1}{U^3V} \tag{4.58}$$

is UV- and IR-finite.

For the ladder diagram in Fig. 4(d) we have

$$\begin{aligned} F_0 &= 4[8A_2(1-A_1+A_1^2)+(1+A_2^2)(1-4A_1+A_1^2)] , \\ F_1 &= 4[B_{11}(1-16A_2+A_2^2)+B_{22}(1-4A_1+A_1^2) \\ &\quad +4B_{12}(1-2A_1+4A_2-2A_1A_2)] , \\ F_2 &= 4(B_{11}B_{22}+5B_{12}^2) . \end{aligned} \tag{4.59}$$

We find

$$L_l = \hat{L}_l + \hat{L}_2\Delta' L_2 + I_l + \Delta L_l , \tag{4.60}$$

where

$$\begin{aligned} I_l &= \tfrac{1}{16}\int dz\,\frac{F_0}{U^2V^2} , \\ \Delta L_l &= \tfrac{1}{16}\int dz(1-K_S)\frac{F_1}{U^3V} . \end{aligned} \tag{4.61}$$

Exactly in parallel with (4.42) we find

$$I_b + I_l + 2I_s = -\tfrac{1}{16}\int dz_b(1-K_S)\frac{H}{U^2V^2} , \tag{4.62}$$

where H is defined by (4.40) with

$$\begin{aligned} H^{(1)} &= H^{(3)} = 4(-2+4A_1-2A_2+A_1A_2) , \\ H^{(2)} &= 4(1-4A_1+A_1^2) . \end{aligned} \tag{4.63}$$

Note that $K_S[z_2(1-A_2^2)H^{(2)}/(U^2V^2)]=0$ so that (4.62) is consistent with the definition (4.61) of I_l.

This time, however, the right-hand side of (4.62) still contains an IR divergence associated with the photon 7, as is easily seen by examining the behavior of the integrand of (4.62) for

$$\begin{aligned} z_7 &= 1-\delta \to 1 , \\ z_{13} &= 0(\delta) , \\ z_{26} &= 0(\epsilon) , \quad \epsilon \simeq \delta^2 . \end{aligned} \tag{4.64}$$

To isolate such divergences we have introduced in II and Sec. II an operation $I_{G/S}$ analogous to K_S. For $S=\{2,6\}$, the $I_{G/S}$ operation consists of the following steps (here we set $G/S \equiv T$):

(b′) $U \to z_7 z_{26}$, $1-A_1 \to z_{13}/z_7$, $A_2 \to z_6/z_{26} \equiv A_2^S$, $V \to V_S + z_{13}^2/z_7$;

(c′) $U \to z_{137} z_{26}$, $V \to V_S + V_T$,

$$\begin{aligned} &-z_2(1-A_2^2)H^{(2)} \\ &\quad \to 2z_2[1-(A_2^S)^2](-2)[1-4A_1^T+(A_1^T)^2] \\ &\quad = F_0[\Delta B_S]\,F_0[L_T] ; \end{aligned}$$

(d′) $$I_T\left[\frac{-z_2(1-A_2^2)H^{(2)}}{U^2V^2}\right] = \frac{F_0[\Delta B_S]F_0[L_T]}{z_{26}^2 z_{137}^2 (V_S+V_T)^2} . \tag{4.65}$$

In step (c′) we have omitted $H^{(1)}$ and $H^{(3)}$ terms since they are IR-finite:

$$I_T(1-K_S)[z_1(1-A_1^2)H^{(1)}] = O(\delta^3) . \tag{4.66}$$

The UV- and IR-finite part of B_b may thus be defined by

$$\Delta B_b = -\tfrac{1}{16}\int dz\left\{(1-K_S)\left[\frac{E_0}{U^2V}-\frac{z_{13}(1-A_1^2)H^{(1)}}{U^2V^2}+\frac{2GF_1}{U^3V}\right]+(1-I_T)\left[\frac{-z_2(1-A_2^2)H^{(2)}}{U^2V^2}\right]\right\} . \tag{4.67}$$

In the limit (4.64) IR divergences might also appear in other integrals such as (4.61). However, this is prevented by relations similar to (4.66), which arise from step (c′) in the definition of $I_{G/S}$.

Factorizing the integral over (4.65) as before we obtain

$$I_T\left[-\tfrac{1}{16}\int dz(1-K_S)\frac{H}{U^2V^2}\right]=I_2\Delta B_2\,. \tag{4.68}$$

We may therefore write

$$\Delta' B_b=\Delta B_b-2I_s-I_1+I_2\Delta B_2\,. \tag{4.69}$$

V. MAGNETIC MOMENT

Parametric integrals for the magnetic moment M are slightly more complicated than those of the charge form factor because of the more elaborate trace projection (2.2) and the appearance of additional scalar currents a_i reflecting the q (momentum transfer) dependence.

As is seen from (2.9), M has no overall UV divergence. Furthermore M is free from *overall* IR divergence as is shown in II.

Let us begin by expressing the second-order magnetic moment $M^{(2)}\equiv M_2$, Fig. 4(b), in our notation

$$M_2=-\tfrac{1}{4}\int dz\,\frac{F_0}{U^2V}\,, \tag{5.1}$$

with

$$F_0=-4A_1(1-A_1)\,, \tag{5.2}$$

where all parametric functions have already been defined in Sec. III. The scalar currents a_i, defined by $Q_i'=A_i\,p+a_i\,q$, have canceled themselves in (5.1) because of the first Kirchhoff's law $a_1'=a_1+1$. M_2 has no IR divergence because of the factor $1-A_1$ in F_0. Carrying out the integration of (5.1) we obtain the familiar result

$$a^{(2)}=M_2=\tfrac{1}{2}\,. \tag{5.3}$$

In the fourth order UV and IR divergences arise from various subdiagrams. Let us first consider the contribution M_l of the ladder diagram in Fig. 4(d):

$$M_l=\tfrac{1}{16}\int dz\int_{\lambda^2}^{\Lambda^2} z_6\,dm_6^{\,2}\left(\frac{2F_0}{U^2V^3}+\frac{F_1}{U^3V^2}\right), \tag{5.4}$$

where

$$\begin{aligned}F_0&=8[(1-A_1)(A_1-3A_2)+A_2(1-3A_1)(A_1-A_2)]\,,\\ F_1&=8[B_{12}(9A_1-10A_2+A_1A_2)+B_{22}A_1(1-A_1)]\,.\end{aligned} \tag{5.5}$$

F_0 vanishes for $A_1,\ A_2\to 1$ so that M has no overall IR divergence. The UV divergence from the subvertex $S=\{2,2',6\}$ can be separated by the K_S operator which yields

$$M_l=\hat{L}_2M_2+\Delta' M_l\,, \tag{5.6}$$

where

$$\Delta' M_l=\tfrac{1}{16}\int dz\left[\frac{F_0}{U^2V^2}+(1-K_S)\frac{F_1}{U^3V}\right]. \tag{5.7}$$

On the other hand, the renormalized contribution to the anomaly is

$$a_l=M_l-L_2M_2\,, \tag{5.8}$$

analogous to (2.9). Substituting (5.6) in (5.8) and recalling (3.14) we find

$$a_l=\Delta' M_l-\Delta' L_2M_2\,. \tag{5.9}$$

This is an example of the general result (2.21).

$\Delta' M_l$ still contains an IR divergence from the $z_7\to 1$ region. This can be isolated by an $I_{G/S}$ operation where $G/S=\{1,3,7\}$:

$$\begin{aligned}\Delta' M_l&=\Delta M_l+I_2M_2\,,\\ \Delta M_l&=\tfrac{1}{16}\int dz\left[(1-I_{G/S})\frac{F_0}{U^2V^2}+(1-K_S)\frac{F_1}{U^3V}\right].\end{aligned} \tag{5.10}$$

Combining this with (5.9) and (3.15) we obtain

$$a_l=\Delta M_l\,. \tag{5.11}$$

Contributions from the remaining fourth-order vertex diagrams can all be written in the form (5.4), where

$$\begin{aligned}F_0&=-8A_1(1-A_1)^2(2+A_2)\,,\\ F_1&=8B_{11}(6A_1-6A_2+4A_1A_2)\end{aligned} \tag{5.12}$$

for the self-energy insertion diagram s,

$$\begin{aligned}F_0&=2A_1A_2(1+A_2)^2-A_1^{\,2}(1+A_2+2A_2^{\,2})\\ &\quad-A_2^{\,2}(3+A_2)+(2a_1-a_2)(1-A_2^{\,2})\,,\\ F_1&=2B_{11}A_2(1+2A_2)\\ &\quad+B_{12}(2+A_1-7A_2+4A_1A_2-6A_2^{\,2}+5a_2)\\ &\quad-B_{22}(1+A_1-3A_2+2A_1A_2-a_1+3a_2)\,,\end{aligned} \tag{5.13}$$

with

$$\begin{aligned}a_1&=-(z_2B_{12}/2+z_3B_{13})/U\,,\\ a_2&=-(z_2B_{22}/2+z_3B_{23})/U\end{aligned} \tag{5.14}$$

for the crossed-ladder diagram x, and

$$\begin{aligned}F_0&=2A_3(1-A_3)(1-A_1A_2)+(1-A_3^{\,2})(4a_1+2a_3)\,,\\ F_1&=2B_{12}A_3(1-A_3)+B_{13}(4A_1+4A_3-8A_2A_3+10a_3)\\ &\quad+2B_{33}(1+A_1A_2+a_1+2a_3)\,,\end{aligned} \tag{5.15}$$

with

$$a_1=-z_3B_{13}/U,\quad a_3=-z_3B_{33}/U \tag{5.16}$$

for the corner diagram c.

Unrenormalized integrals and K-finite parts of these contributions are IR-finite. However, IR divergences appear in the renormalized expressions through the subtraction terms. Separating out the UV divergences of diagrams c and s by K_S operation, we find

$$a_s = \Delta M_s - \Delta' B_2 M_2 ,$$
$$a_c = \Delta M_c - \Delta' L_2 M_2 , \qquad (5.17)$$
$$a_x = M_x .$$

In the sixth order most traces become too lengthy to evaluate manually. We have evaluated only a few of them by hand. They were useful for testing our computer programs by which all traces have been evaluated. Since the magnetic-moment projection (2.2) involves products of up to 16 γ matrices and could generate more than 3^9 terms in the intermediate stages, very careful programming was needed. We have worked this out in two different ways: (1) We have generated all integrands using the SCHOONSCHIP algebraic computation program of Veltman[29] at the CDC-6600 computer of Brookhaven National Laboratory.

(2) We have also developed a program[30] combining TECO and REDUCE 2 suited to the PDP-10 computer at the Wilson Electron Synchrotron Laboratory at Cornell University. Some outputs of SCHOONSCHIP were doublechecked by this approach. Furthermore, results of trace calculation for all individual diagrams of Fig. 2 have been shown to agree with the corresponding expressions of Levine and Wright.[31] Additional checks have been provided by K_S and $I_{G/S}$ operations which reduce the integrands to known lower-order expressions.

Typical integrands thus generated consist of as many as 500 terms (though this may be shortened by judicious use of Kirchhoff's laws and appropriate factorizations). To illustrate our general approach, let us examine some representative diagrams in detail.

The simplest diagram is $A1$ of Fig. 2 which contains two second-order self-energy insertions. The parametric integral for $A1$ is given by (see Fig. 5 for notation)

$$M_{A1} = -\tfrac{1}{32}\int dz \left(\frac{F_0}{U^2V^3} + \frac{F_1}{2U^3V^2} + \frac{F_2}{2U^4V} \right), \qquad (5.18)$$

with

$$F_0 = -16A_1(1-A_1)^3(2+A_2)(2+A_4),$$
$$F_1 = -16A_1[4B_{11}(-9+4A_1)+2(B_{12}+B_{14})(9-12A_1+8A_1^2)-B_{24}(3-12A_1+24A_1^2-10A_1^3)], \qquad (5.19)$$
$$F_2 = 64B_{11}A_1[B_{24}(-9+5A_1)+6(B_{12}+B_{14})] .$$

M_{A1} has no IR divergence. UV divergences from $S=\{2, 6\}$ and $S'=\{4, 7\}$ can be removed by K operations. Defining the UV- (and IR-) finite part by

$$\Delta M_{A1} = -\tfrac{1}{32}\int dz (1-K_S)(1-K_{S'})\left[\frac{F_0}{U^2V^3} + \frac{1}{2}\left(\frac{F_1}{U^3V^2} + \frac{F_2}{U^4V} \right) \right] \qquad (5.20)$$

we can write (5.18) as

$$M_{A1} = \Delta M_{A1} + 2\delta m_2 M_{A1*} + 2\hat{B}_2 M_s - (\delta m_2)^2 M_{A1**}$$
$$-2\delta m_2 \hat{B}_2 M_{2*} - (\hat{B}_2)^2 M_2 , \qquad (5.21)$$

where the diagrams $A1*$ and $A1**$ are defined in Fig. 5. Taking account of mass counterterms and renormalizations in Table VI, we may thus express the renormalized contribution to the anomaly as

$$a_{A1} = \Delta M_{A1} - 2\Delta' B_2 (M_s - \delta m_2 M_{2*})$$
$$+ [2\hat{B}_2 \Delta' B_2 + (\Delta' B_2)^2] M_2$$
$$= \Delta M_{A1} - 2\Delta' B_2 \Delta M_s + (\Delta' B_2)^2 M_2 . \qquad (5.22)$$

The second and third terms are known from lower-order calculations. Thus we have only to evaluate ΔM_{A1} to obtain a_{A1}. The result (5.22) is an example of the general formula (2.21).

The integral for the diagram $A2$ of Fig. 2 is given by (5.18) with appropriately redefined F_0, F_1, F_2. This integral has UV divergences from the vertex part $S=\{2, 2', 6\}$ and self-energy part $S'=\{4, 7\}$. If we define the UV-finite part of M_{A2} by

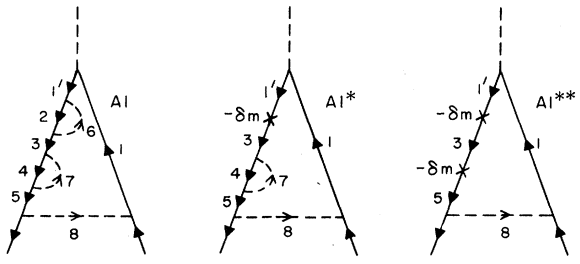

FIG. 5. Diagram $A1$ and its self-mass counterterms $A1*$ and $A1**$.

$$\Delta' M_{A2} = -\tfrac{1}{32}\int dz(1-K_{S'}) \times\left[\frac{F_0}{U^2V^3} + \tfrac{1}{2}(1-K_S)\left(\frac{F_1}{U^3V^2} + \frac{F_2}{U^4V}\right)\right], \tag{5.23}$$

we find

$$M_{A2} = \Delta' M_{A2} + \delta m_2 M_{A2*} + \hat{B}_2 M_1 + \hat{L}_2(M_s - \delta m_2 M_{2*}) - \hat{L}_2\hat{B}_2 M_2 . \tag{5.24}$$

This time $\Delta' M_{A2}$ is still IR-divergent. The separation of the IR-divergent part of (5.23) can be achieved by an $I_{G/S}$ operation

$$\Delta' M_{A2} = \Delta M_{A2} + I_s M_2 , \tag{5.25}$$

where I_s is defined by (4.57), $G/S = \{1, 3, 4, 5, 7, 8\}$, and

$$\Delta M_{A2} = -\tfrac{1}{32}\int dz(1-K_{S'})\left[(1-I_{G/S})\frac{F_0}{U^2V^3} + \tfrac{1}{2}(1-K_S)\left(\frac{F_1}{U^3V^2} + \frac{F_2}{U^4V}\right)\right] \tag{5.26}$$

is the completely finite expression ready for numerical integration.

Diagrams $D4$ and $E3$ have similar fourth-order IR divergences which can be separated in the same fashion:

$$\Delta' M_{D4} = \Delta M_{D4} + I_c M_2 , \tag{5.27}$$

$$\Delta' M_{E3} = \Delta M_{E3} + I_x M_2 . \tag{5.28}$$

The IR structure of the diagram $B3$ is more complicated. We shall postpone the analysis of $B3$ till later.

Some diagrams have IR divergence arising from a single photon. For instance, the diagram $C3$ has an IR divergence in the limit $z_8 \to 1$. This divergence can be separated by an $I_{G/S}$ operation, $G/S = \{1, 5, 8\}$, which yields

$$I_{G/S}\Delta' M_{C3} = I_2 M_x , \tag{5.29}$$

where M_x is given by (5.13) and (5.14). The UV- and IR-finite part of M_{C3} is given by

$$\Delta M_{C3} = -\tfrac{1}{32}\int dz\left[(1-I_{G/S})\left(\frac{F_0}{U^2V^3} + \frac{F_1}{2U^3V^2}\right) + \tfrac{1}{2}(1-K_S)\frac{F_2}{U^4V}\right] . \tag{5.30}$$

Analogously we obtain

$$I_{G/S}\Delta' M_{B2} = I_2 \Delta M_s ,$$
$$I_{G/S}\Delta' M_{B3} = I_2 \Delta' M_1 , \tag{5.31}$$
$$I_{G/S}\Delta' M_{C2} = I_2 \Delta M_c .$$

Some diagrams contain UV divergences arising from fourth-order subdiagrams. Let us first consider the fourth-order vertex part $S = \{2, 3, 4, 5, 7, 8\}$ of diagram $H1$. By (2.18) this UV divergence is confined to the F_2 term. Furthermore only those terms of F_2 obtained by contractions of lines 2, 3, 4, 5 contribute. They factor as

$$K_S F_2 = F_2[L_S]F_0[M_{G/S}] , \tag{5.32}$$

where $F_2[L_S]$ and $F_0[M_{G/S}]$ are defined by (4.27) and (5.2), respectively. This leads to the factorization of M_{H1}:

$$K_S M_{H1} = \hat{L}_x M_2 , \tag{5.33}$$

where $\hat{L}_x$ is defined by (4.28). Fourth-order vertex divergences from the diagrams $B2$, $B3$, $C2$, $C3$, $D1$, $E1$, $F1$, $G1$, and $G5$ can be handled in a similar fashion.

Let us now consider diagrams containing fourth-order self-energy subdiagrams. For instance, the diagram $C1$ has a UV-divergent subdiagram $S_1 = \{2, 3, 4, 6, 7\}$. It is easily seen that this divergence is confined to F_1 and F_2 terms; further, only those terms containing B_{23}, B_{24}, or B_{34} contribute. In step (b) of the K_{S_1} operation we need relations like

$$K_{S_1} B_{mj} = z_{11'58} A_m^{S_1} U^{S_1} ,$$
$$K_{S_1} B_{mn} = z_{11'58} B_{mn}^{S_1} , \quad m, n \in S_1 ,$$
$$K_{S_1} A_m = A_m^{S_1} A_1^{G/S_1} , \quad j = 1, 1', 5 , \tag{5.34}$$
$$K_{S_1} A_j = A_1^{G/S_1} ,$$

which follow from (I.91) and (I.93).

The diagram $C1$ is the only one in Fig. 2 that contains overlapping UV subdivergences; vertex parts $S_2 = \{2, 3, 7\}$ and $S_3 = \{3, 4, 6\}$ have the line 3 in common. However, as is shown in (II.2.26), this causes no problem because of the identity

$$(1-K_{S_1})K_{S_2}K_{S_3} = 0, \quad S_1 = S_2 \cup S_3 . \tag{5.35}$$

Carrying out all K_S operations we obtain

$$a_{C1} = \Delta M_{C1} - \Delta'\delta m_a M_{2*} - 2\Delta' L_2 \Delta M_s - \Delta' B_a M_2 + 2\Delta' B_2 \Delta' L_2 M_2 , \tag{5.36}$$

where

$$\Delta M_{C1} = -\tfrac{1}{32}\int dz\left[\frac{F_0}{U^2V^3} + \tfrac{1}{2}(1-K_{S_1})(1-K_{S_2}-K_{S_3})\left(\frac{F_1}{U^3V^2} + \frac{F_2}{U^4V}\right)\right] . \tag{5.37}$$

Finally let us examine the diagram $B3$ which contains IR divergences arising from two sources, $G/S_1 = \{1, 5, 8\}$ and $G/S_2 = \{1, 2, 4, 5, 7, 8\}$. The IR-finite part is given by

$$\begin{aligned}\Delta M_{B3} &= (1-I_{G/S_1})(1-I_{G/S_2})\Delta' M_{B3} \\ &= \Delta' M_{B3} - I_1 M_2 - I_2 \Delta' M_1 + I_2^2 M_2 ,\end{aligned} \tag{5.38}$$

where I_i and $\Delta' M_i$ are given by (4.61) and (5.10), respectively. Of all diagrams in Fig. 2, this one requires the largest number of subtraction terms. It is instructive to display ΔM_{B3} in a fully expanded form:

$$\begin{aligned}\Delta M_{B3} = -\tfrac{1}{32}\int dz \Big[& \frac{F_0}{U^2V^3} + \frac{1}{2}\left(\frac{F_1}{U^3V^2} + \frac{F_2}{U^4V}\right) \\ & - I_{G/S_2}\frac{F_0}{U^2V^3} - \frac{1}{2}K_{S_2}\left(\frac{F_1}{U^3V^2} + \frac{F_2}{U^4V}\right) \\ & - I_{G/S_1}\left(\frac{F_0}{U^2V^3} + \frac{F_1}{2U^3V^2}\right) - K_{S_1}\frac{F_2}{2U^4V} \\ & + I_{G/S_1}I_{G/S_2}\frac{F_0}{U^2V^3} + K_{S_2}I_{G/S_1}\frac{F_1}{2U^3V^2} + K_{S_1}K_{S_2}\frac{F_2}{2U^4V}\Big] ,\end{aligned} \tag{5.39}$$

where $S_1 = \{2, 3, 3', 4, 6, 7\}$ and $S_2 = \{3, 3', 6\}$. Note that, by the definitions of K_S and $I_{G/S}$ operations given in Sec. II, the functions U and V for all terms in *each line* of (5.39) are redefined in the same way.

This example shows how to construct finite integrals explicitly for all diagrams of Fig. 2. In most cases the structure of the integrand is considerably simpler.

By rewriting renormalized expressions $M_i + r_i$ [see (2.10) and Table VI] in terms of their K-finite parts, we can verify directly the general formula (2.21); replace each term in the Dyson-Salam expression for renormalized amplitude by its K-finite part. Noting further simplifications

$$\begin{aligned}&\Delta'\delta m_2 = 0, \quad \Delta'\delta m_{a,b} = \Delta\delta m_{a,b} , \\ &\Delta' M_2 = M_2 , \quad \Delta' M_{2*} = M_{2*} = M_2 , \quad \Delta' M_{x,c,s} = \Delta M_{x,c,s}\end{aligned} \tag{5.40}$$

we obtain the K-renormalized expressions listed in Table VI. Since these expressions are still IR-divergent, we reexpress in Table I all entries in terms of UV- and IR-finite integrals and corresponding IR-divergent constants. Noting that IR-divergences cancel within each internally gauge-invariant set of diagrams,[32] we have regrouped our results accordingly. (In our way of numbering the diagrams, diagram $A1$ belongs to the externally gauge-invariant set A, and the internally gauge-invariant set 1. All the sets are A, B, C, D, $\overline{D}$, E, F, G, $\overline{G}$, H and 1, 2, 3, 3′, 4, 5, respectively. By the time-reversal invariance $D = \overline{D}$, $G = \overline{G}$, $1 = 5$, and $2 = 4$. 3 and 3′ differ by the number of virtual photons crossing the external vertex.) Table I also contains the result of numerical evaluation of $\eta_i \Delta M_i$ where $\eta_i = 1$ if the diagram is symmetric under time reversal and $= 2$ otherwise.[33]

Summing all terms of Table I yields

$$\begin{aligned}a_4^{(6)} = & \sum_i \eta_i \Delta M_i - 4\Delta B_2 \Delta M^{(4)} \\ & - (3\Delta L^{(4)} + 2\Delta\delta m^{(4)} + 2\Delta B^{(4)})M_2 + 5(\Delta B_2)^2 M_2 ,\end{aligned} \tag{5.41}$$

where ΔB_2, M_2 are given by (3.26) and (5.3), and

$$\begin{aligned}\Delta M^{(4)} &= M_x + 2\Delta M_c + \Delta M_l + 2\Delta M_s , \\ \Delta L^{(4)} &= \Delta L_x + 2\Delta L_c + \Delta L_l + 2\Delta L_s , \\ \Delta\delta m^{(4)} &= \Delta\delta m_a + \Delta\delta m_b , \\ \Delta B^{(4)} &= \Delta B_a + \Delta B_b .\end{aligned} \tag{5.42}$$

Note that (5.41) is somewhat simpler than (2.11). This is due to our definition of I_2 in (3.15) which sets $\Delta L_2 = 0$.

We list the numerical values of all fourth-order integrals contributing to (5.41) in Table II. The first eight entries are known analytically, and although analytic evaluation of the rest presents no difficulty, we have not done so for lack of time. Combining the results in Tables I and II we obtain

$$a_4^{(6)}(\text{individual}) = 0.943(32) \tag{5.43}$$

as the contribution of 50 diagrams of group 4 to the electron anomaly. The errors from independent diagrams are combined statistically.

VI. ALTERNATIVE APPROACH

In drawing the diagrams of Fig. 2 we have emphasized that they are all derived from the self-energy diagrams of Fig. 3 by inserting an external vertex in all possible ways. Vertex diagrams derived from the same self-energy diagram share

many properties. In fact, in the limit $q=0$, they have common functions U, V, B_{ij}, and A_i so that it is natural to treat them collectively. (Only the scalar currents a_i associated with q are not common.) In this section we go even further and amalgamate these integrals into a single one using the Ward-Takahashi identity. In the end this approach reduces the number of independent integrals from 28 to 8, enabling us to save considerable time and effort of computation.

As is well known, proper vertex and self-energy parts are related by the Ward-Takahashi identity

$$q_\mu \Lambda^\mu(p,q) = -\Sigma(p+q/2) + \Sigma(p-q/2) , \tag{6.1}$$

where we have set $\Gamma^\mu = \gamma^\mu + \Lambda^\mu$. This identity holds not only for the exact Σ and Λ but also for perturbation-theoretical Σ_G and Λ_G, where Σ_G is calculated from an electron self-energy diagram G and Λ_G is the sum of vertex diagrams obtained by inserting an external vertex in G in all possible ways. Differentiating both sides of (6.1) with respect to q^μ and dropping terms quadratic or higher in q, we obtain

$$\Lambda^\nu(p,q) \simeq -q^\mu \left[\frac{\partial \Lambda_\mu(p,q)}{\partial q_\nu}\right]_{q=0} - \frac{\partial \Sigma(p)}{\partial p_\nu} . \tag{6.2}$$

This is the starting point of our consideration.

If we set $q=0$ in (6.2), we recover the familiar Ward identity (2.4). It is instructive to examine how (2.4) is realized in the parametric space. As an example we shall show that

$$L_x + 2L_c = -B_a . \tag{6.3}$$

For this purpose it is convenient to parametrize the integrals for L_x and L_c in a slightly different fashion. [See Fig. 4(d).] First, we note the identity

$$\frac{(\not p_i + m_i)\gamma^\nu(\not p_i + m_i)}{(p_i^2 - m_i^2)^2} = 2D_i^\nu(\not\Phi_i + m_i)\frac{1}{(p_i^2 - m_i^2)^2} , \tag{6.4}$$

which follows from

$$\frac{p_i^\mu p_i^\nu}{(p_i^2 - m_i^2)^2} = D_i^\mu D_i^\nu \frac{1}{(p_i^2 - m_i^2)^2} + \frac{g^{\mu\nu}}{2(p_i^2 - m_i^2)} , \tag{6.5}$$

where D_i^μ is defined in (3.2). As is seen from the Feynman formula (I.19), repeating the denominator $(p_i^2 - m_i^2)^{-1}$ will lead to the appearance of the z_i factor after parametrization. If we now parametrize L_x according to the procedure of I Sec. III, we find from (6.4)

$$L_x = \tfrac{1}{16}\int dz\, 2z_2 p_\nu D_2^\nu \mathsf{F}\frac{1}{U^2V^2} , \tag{6.6}$$

where p_ν is part of the projection operator in (2.3) and F, dz, U, V are all defined for the self-energy diagram a of Fig. 4(c). Parametrizing the two L_c diagrams in the same way we obtain

$$L_x + 2L_c = \tfrac{1}{16}\int dz\, p_\nu \left(\sum_{i=1}^{3} 2z_i D_i^\nu\right) \mathsf{F}\frac{1}{U^2V^2} . \tag{6.7}$$

Let us now carry out D_i^ν operations. The term in the parentheses contracted with any $\not\Phi_j$ in F gives

$$\sum_{i=1}^{3} 2z_i(pD_i)\not\Phi_j \frac{1}{U^2V^n}\Bigg|_{\text{contracted}} = \not p\left(-\frac{1}{U}\sum_{i=1}^{3} z_i B'_{ij}\right)\frac{1}{n-1}\frac{1}{U^2V^{n-1}} = \frac{A_i \not p}{(n-1)U^2V^{n-1}} , \tag{6.8}$$

taking account of (I.37) and (I.74). On the other hand, if D_i^ν is not contracted, we obtain

$$\sum_{i=1}^{3} 2z_i(p\cdot D_i)\frac{1}{V^n} = \frac{2G}{V^n} , \tag{6.9}$$

G being defined by (I.36). Thus we find

$$L_x + 2L_c = \tfrac{1}{16}\int dz\left(\mathsf{E}\frac{1}{U^2V} + 2G\,\mathsf{F}\frac{1}{U^2V^2}\right) , \tag{6.10}$$

where E is defined by (2.17). As is seen from (2.16) this is identical with $-B_a$, verifying (6.3). This argument is generalizable to any order. It hinges on the relation (6.4) which is applicable to any vertex in which external q^μ vanishes.

Let us now consider the extraction of magnetic-moment term from (6.2). For this purpose it is convenient to deviate from the convention of (I.10) slightly and exhibit the dependence on the external momentum q explicitly. Namely, let us denote the electron momenta as

$$p_j \pm q/2 \text{ if } j \text{ is an electron line to the } \begin{pmatrix}\text{left}\\ \text{right}\end{pmatrix} \text{of the external vertex} , \tag{6.11}$$

while the photon momenta are unchanged. p_j is then a linear combination of the external electron momentum p and integration variables r_k.

Before parametrizing $q_\mu(\partial\Lambda^\mu/\partial q_\nu)$ in (6.2), let us carry out the differentiation with respect to q_ν explicitly using (6.4) and the identities

$$\left[\frac{\partial}{\partial q_\nu}\frac{1}{\not p \pm \not q/2 - m}\right]_{q=0} = \mp\frac{1}{2}\frac{(\not p+m)\gamma^\nu(\not p+m)}{(p^2-m^2)^2},$$
$$\left[\frac{\partial}{\partial q_\nu}\left(\frac{1}{\not p+\not q/2-m}\gamma^\mu\frac{1}{\not p-\not q/2-m}\right)\right]_{q=0} = -\frac{1}{2}\frac{\gamma^\mu\gamma^\nu(\not p+m)-(\not p+m)\gamma^\nu\gamma^\mu}{(p^2-m^2)^2}. \tag{6.12}$$

For instance, for the integrand of $\Lambda_3^\mu \equiv \Lambda_c^\mu(p,q)$ for the corner diagram, we obtain

$$\left[\frac{\partial}{\partial q_\nu}\left(\gamma^\alpha\frac{1}{\not p_3+\not q/2-m_3}\gamma^\mu\frac{1}{\not p_3-\not q/2-m_3}\gamma^\beta\frac{1}{\not p_2-\not q/2-m_2}\gamma_\alpha\frac{1}{\not p_1-\not q/2-m_1}\gamma_\beta\right)\right]_{q=0}$$
$$= -\left(\mathsf{Z}_3^{\mu\nu}+2\sum_{j=1}^{3}\epsilon_{3j}D_3^\mu D_j^\nu \mathsf{F}\frac{1}{p_j^2-m_j^2}\right)\frac{1}{(p_3^2-m_3^2)\prod_{i=1}^{3}(p_i^2-m_i^2)}, \tag{6.13}$$

where

$$\epsilon_{ij} = -\epsilon_{ji} = 1 \text{ if } i<j, \tag{6.14}$$

and $\mathsf{Z}_3^{\mu\nu}$ is obtained from F by replacing $(\not p_3+m_3)$ by $[\gamma^\mu\gamma^\nu(\not p_3+m_3)-(\not p_3+m_3)\gamma^\nu\gamma^\mu]/2$.

If we now parametrize $q_\mu(\partial\Lambda_3^\mu/\partial q_\nu)$ according to the method of I Sec. III, we find

$$-q_\mu\left[\frac{\partial\Lambda_3^\mu}{\partial q_\nu}\right]_{q=0} = \tfrac{1}{16}q_\mu\int dz\left(z_3\mathsf{Z}_3^{\mu\nu}\frac{1}{U^2V^2}-4\sum_{j=1}^{3}\epsilon_{3j}D_3^\mu D_j^\nu\mathsf{F}\frac{z_3z_j}{U^2V^3}\right). \tag{6.15}$$

Similar results are obtained for the crossed-ladder diagram Λ_2^μ and the other corner diagram Λ_1^μ. Summing up these contributions we get

$$-q_\mu\left[\frac{\partial\Lambda_a^\mu}{\partial q_\nu}\right]_{q=0} = \tfrac{1}{16}\int dz\left(\mathsf{Z}^\nu\frac{1}{U^2V^2}-4q_\mu\sum_{i,j=1}^{3}\epsilon_{ij}D_i^\mu D_j^\nu\mathsf{F}\frac{z_iz_j}{U^2V^3}\right), \tag{6.16}$$

where $\Lambda_a^\mu = \Lambda_1^\mu+\Lambda_2^\mu+\Lambda_3^\mu$ and

$$\mathsf{Z}^\nu = q_\mu\sum_{j=1}^{3}z_j\mathsf{Z}_j^{\mu\nu}. \tag{6.17}$$

In projecting out the magnetic-moment contribution of (6.16), it is seen that the only contributions arise from the case where D_i^μ and D_j^ν are both contracted with the $\not p_k$ operators within F. Thus the magnetic part of (6.16) can be written as

$$\tfrac{1}{16}\int dz\left(\mathsf{Z}^\nu\frac{1}{U^2V^2}-\frac{1}{2U^2}\sum_{i,j,k,l}^{1,2,3}\epsilon_{ij}z_iz_jB'_{ik}B'_{jl}q_\mu\mathsf{F}_{kl}^{\mu\nu}\frac{1}{U^2V}\right), \tag{6.18}$$

where $\mathsf{F}_{kl}^{\mu\nu}$ is obtained from F by replacing $(\not p_k+m_k)$ and $(\not p_l+m_l)$ by γ^μ and γ^ν, respectively.

This result can be easily generalized to any self-energy diagram G and associated vertex diagrams. For simplicity let us define

$$\mathsf{C}^\nu = q_\mu\sum_{i<j}C_{ij}\mathsf{F}_{ij}^{\mu\nu}, \tag{6.19}$$

where

$$C_{ij} = -\frac{1}{U^2}\sum_{k=1}^{2n-2}\sum_{l=k+1}^{2n-1}z_kz_l(B'_{ik}B'_{jl}-B'_{il}B'_{jk}). \tag{6.20}$$

Then we find

$$-q_\mu\left[\frac{\partial\Lambda_G^\mu}{\partial q_\nu}\right]_{\text{mag. mom. part}} = \left(\frac{-1}{4}\right)^n(n-1)!\int dz\left[\mathsf{Z}^\nu\frac{1}{U^2V^n}+\mathsf{C}^\nu\frac{1}{(n-1)U^2V^{n-1}}\right], \tag{6.21}$$

taking account of $\mathsf{F}_{kl}^{\mu\nu} = -\mathsf{F}_{lk}^{\mu\nu}$. If we now project out the magnetic-moment term from (6.21) and the second term of (6.2) with the help of (2.2), we finally obtain

$$M_G^{(2n)} = \left(\frac{-1}{4}\right)^n (n-1)! \int dz \left[\frac{\mathsf{E}+\mathsf{C}}{n-1} \frac{1}{U^2 V^{n-1}} + (2\mathsf{GF}+\mathsf{Z}) \frac{1}{U^2 V^n} \right] \tag{6.22}$$

as the contribution to the electron anomaly from all vertex diagrams associated with the self-energy diagram G of order $2n$. E, C, F, Z are magnetic projections of E^ν, C^ν, $p^\nu\mathsf{F}$, Z^ν, respectively.

The integrand of (6.22) looks more complicated than those of individual vertex diagrams. However, actual trace calculation is much simpler because only C^ν and Z^ν depend on q, and that in a very simple fashion. After the trace calculation is carried out, the numerators turn out to be of similar lengths as those of individual vertex diagrams. Since each integral of the form (6.22) replaces $2n-1$ individual integrals, this application of Ward-Takahashi identity amounts to a manifold reduction in the time and effort of computation.

In (6.22) parametric functions C_{ij} replace scalar currents a_i in individual vertex contributions. Calculation of C_{ij} is greatly facilitated by the topological formula discussed in I Sec. IV G. This calculation is trivial in the fourth order. Since it becomes fairly tedious in the sixth order, however, we have computed them on the PDP-10 computer, using TECO and REDUCE-2. Note also that C_{ij} are related to each other by relations derived from Kirchhoff's laws for B_{ij}. These relations are useful for their computation and crosschecking. In the Appendix we give examples of computation of C_{ij}.

As an illustration of (6.22) we give explicit formulas for the fourth-order magnetic moments M_a and M_b associated with the self-energy diagrams a and b of Fig. 4(c). M_a is of the form

$$M_a = \tfrac{1}{16} \int dz \left(\frac{E_0+C_0}{U^2 V} + \frac{2GF_0+Z_0}{U^2 V^2} + \frac{2GF_1+Z_1}{U^3 V} \right) , \tag{6.23}$$

where

$$\begin{aligned}
E_0 &= 8(2A_1A_2A_3 - A_1A_2 - A_1A_3 - A_2A_3) , \\
C_0 &= -8(C_{21}+C_{31}+C_{32}) = -24 z_6 z_7 / U , \\
F_0 &= \tfrac{1}{2} E_0 - 4(A_1+A_2+A_3-2) , \\
Z_0 &= 8z_1(-A_1+A_2+A_3+A_1A_2+A_1A_3-A_2A_3) \\
&\quad + 8z_2(2-A_1+A_2-A_3-A_1A_2 \\
&\qquad + A_1A_3 - A_2A_3 + 2A_1A_2A_3) \\
&\quad + 8z_3(A_1+A_2-A_3-A_1A_2+A_1A_3+A_2A_3) , \\
F_1 &= 4[B_{12}(2-A_3) + 2B_{13}(1-2A_2) + B_{23}(2-A_1)] , \\
Z_1 &= -8z_1[B_{23}A_1 - B_{12}A_3 + B_{12} + B_{13}] \\
&\quad + 8z_2[B_{23}(1-A_1) - 4B_{13}A_2 + B_{12}(1-A_3)] \\
&\quad - 8z_3[B_{12}A_3 - B_{23}A_1 + B_{13} + B_{23}] .
\end{aligned} \tag{6.24}$$

The integral for M_b is also given by (6.23) but with

$$\begin{aligned}
E_0 &= 8A_1[4(A_2-A_1) - A_1A_2] , \\
C_0 &= -8A_2 , \\
F_0 &= -4[4(1-A_1+A_1^2) + A_2(1-4A_1+A_1^2)] , \\
Z_0 &= 8z_{13}[4A_1 - A_2(1+A_1^2)] + 8z_2A_2(1+A_1^2) , \\
F_1 &= 32(B_{11}-B_{12}) + 12A_1B_{12} , \\
Z_1 &= 24(z_{13}-z_2)A_1B_{12} .
\end{aligned} \tag{6.25}$$

For the sixth order we have again generated the integrands of (6.22) by SCHOONSCHIP. Renormalization and IR-divergence separation can be carried out by K_S and $I_{G/S}$ operations as before. However, the $I_{G/S}$ operation now requires much more careful treatment than the previous case as a consequence of the use of formulas such as (6.4).[34] We list the renormalization terms for sixth-order calculations in Table VII, and K-renormalized expressions in Table III. The contribution from all diagrams of group 4 is given by[33]

$$\begin{aligned}
a_4^{(6)} &= \sum_i \eta_i \Delta M_i - 3\Delta B_2 \Delta M_g^{(4)} \\
&\quad - (2\Delta L^{(4)} + 2\Delta\delta m^{(4)} + \Delta B^{(4)}) M_2 + 2(\Delta B_2)^2 M_2 ,
\end{aligned} \tag{6.26}$$

where the summation is over all self-energy diagrams of Fig. 3, and all lower order quantities except $\Delta M_g^{(4)}$ are defined in Sec. V. $\Delta M_g^{(4)}$ is given by

$$\Delta M_g^{(4)} = \Delta M_a + \Delta M_b , \tag{6.27}$$

where ΔM_a and ΔM_b are related to the fourth-order quantities defined in Sec. V by

$$\begin{aligned}
\Delta M_a &= M_x + 2\Delta M_c , \\
\Delta M_b &= \Delta M_I + 2\Delta M_s - \Delta B_2 M_2 .
\end{aligned} \tag{6.28}$$

We have evaluated $\Delta M_A, \ldots, \Delta M_H$ numerically using RIWIAD. The result is summarized in Table III. Collecting the results of Table III and Table II we obtain

$$a_4^{(6)}(\text{group}) = 0.893(42) , \tag{6.29}$$

where the error comes mostly from the diagrams B and D. We have not tried to cut down the error of diagram B further for reasons discussed to-

TABLE VII. Subtraction terms for grouped diagrams in the usual renormalization.

Group	$a_i - M_i$
A	$-2B_2(M_b - \delta m_2 M_{2*}) + B_2^2 M_2$
B	$-B_2(M_b - \delta m_2 M_{2*}) - 2(\delta m_b - \delta m_2 \delta m_{2*})M_{2*} - (B_b - \delta m_2 B_{2*})M_2 + B_2^2 M_2$
C	$-2L_2(M_b - \delta m_2 M_{2*}) - 2\delta m_a M_{2*} - B_a M_2 + 2L_2 B_2 M_2$
D	$-L_2(M_b - \delta m_2 M_{2*}) - B_2 M_a - (L_s - \delta m_2 L_{2*})M_2 + 2L_2 B_2 M_2$
E	$-B_2 M_a - 2(L_s - \delta m_2 L_{2*})M_2 + 2B_2 L_2 M_2$
F	$-2L_2 M_a - 2L_c M_2 + 3L_2^2 M_2$
G	$-L_2 M_a - L_1 M_2 - L_c M_2 + 2L_2^2 M_2$
H	$-2L_x M_2$

ward the end of Sec. VII. On the other hand, it would be necessary to use a substantially larger number of subcubes in order to improve the accuracy of the diagram D because of the oscillatory structure of the integrand in the central region.

VII. ANALYSIS OF NUMERICAL RESULTS

We have evaluated the integrals for individual and grouped diagrams prepared in Secs. V and VI using the integration subroutine RIWIAD described in Ref. 7. It is a Monte Carlo integration program with self-adjusting subintervals (or subcubes) which generates an estimate of the integral and a 90% confidence limit of error. A selected set of these values for each integral is then averaged by the maximum-likelihood method. The reliability of our results depends of course on the quality of RIWIAD outputs and the selection criteria.

There are two ways to improve the accuracy of RIWIAD integration: One is to make an appropriate mapping of integration variables, and the other is to increase the number of subcubes and iterations. To proceed systematically we have evaluated each integral in three steps: (1) set-up stage, (2) confirmation stage, and (3) evaluation stage.

Step 1. We typically use 60 000 subcubes and five iterations and try to reduce the "error" of integration by a change of variables of the form

$$y_i = f_i(x_i), \quad 0 \leq x_i \leq 1, \quad 0 \leq y_i \leq 1, \quad i = 1, 2, \ldots, \qquad (7.1)$$

where

$$f_i(x_i) = \frac{\int_0^{x_i} x^m (1-x)^n \, dx}{\int_0^1 x^m (1-x)^n \, dx} \quad . \qquad (7.2)$$

This mapping is designed to stretch the ends ($x_i = 0$ and/or $x_i = 1$), where the integrand grows rapidly, by a suitable choice of non-negative integers m and n. After mapping the integrand will be "flatter" and will lead, with some luck, to a smaller variance. Unfortunately such a mapping will not help if the integrand has a rapidly varying structure in the central region (not on the edges of the unit cube integration domain) or a peak in some direction in the multidimensional domain of integration (other than one along an axis). In such cases it is difficult to obtain a good result by such a simple mapping as (7.1). In our application, however, such mappings have yielded results with reasonably small variance in the majority of cases. A notable exception is the integral for the grouped diagram D whose error we could not bring under control because of an oscillating structure in the central region.

Step 2. In this step we try to check the adequacy of step 1 by increasing the number of subcubes of about 180 000 (with five interations). In most cases the value of the integral is found to stay within the stated error, and the error itself is reduced by $\sim 1/\sqrt{3}$, as is expected. In some cases, however, we have found that the value of the integral had drifted beyond the errors of the step 1. (Integrals $D2$ and $F2$ had such drifts.) In these cases we had to increase the number of subcubes to about 360 000 or even more before no further drift could be detected.

Step 3. We now perform integrations using 360 000 to 1 000 000 subcubes. The limit on the number of subcubes is dictated by the practical restriction on computing time (each job is limited to a maximum of one hour computing time). The number of iterations ranged from 4 to 10. Since the interval structure of the previous run could be used to start the next job, the effective number of iterations was usually larger than 10.

In most cases the values of integrals obtained by steps 1, 2, and 3 were consistent with each other and their errors decreased. We took this as an indication that RIWIAD was giving us reliable results. Still, it is our impression from experience that the errors given by RIWIAD tend to be over-optimistic when the number of subcubes is small. For this reason we decided to use only the results of step 3 in our final analysis.

As was mentioned already, in some cases ($D2$ and $F2$ in particular) the value of the integral obtained with 360 000 subcubes drifted considerably beyond the errors of earlier step. Presumably,

when the number of subcubes is too small, RIWIAD fails to explore some important portion of the domain of integration due to a peculiarity in the mechanism of optimization of axis subdivision. Although such a drift appears to have stopped for 720 000 subcubes, we have not been able to confirm this by running with larger number of subcubes for lack of computing time. For diagrams $F2$ and $D2$ we have included only numbers with 720 000 subcubes in our final results in Table I.

In our preliminary calculation[4] we did not go much beyond step 1 of the above procedure. We evaluated each integral a number of times, changing the mapping of variables each time, but using only relatively small number of subcubes (about 180 000 at most). For each integral many of these values were then averaged by the maximum-likelihood method (using the RIWIAD-supplied errors for weighting) and the compounded error was calculated from $(\sum_i \sigma_i^{-2})^{-1/2}$. Later recomputation of these integrals with larger number of subcubes revealed that the errors thus obtained were too optimistic presumably because in some cases RIWIAD systematically failed to explore certain parts of the domain if the number of subcubes was too small. If we reanalyze the integrals of our preliminary report[4] retaining only those computed with the largest number of subcubes, we find $a_4^{(6)} = 1.008(81)$. In this manner we can remove the apparent discrepancy between the previously reported value 1.02(4) and the result of the present calculation. Different treatments of IR divergences in Ref. 4 and the present paper prevent us from going into more detailed comparison without further computation.

Since we have computed $a_4^{(6)}$ in two independent ways, we are in a position to crosscheck the eight integrals of Sec. VI with the sums of the corresponding vertex diagrams of Sec. V. Such a comparison is shown in Table IV. The agreement is excellent except for the groups B and D, where the differences between the two results are 0.017 and 0.014, respectively. Actually the latter is acceptable since the RIWIAD error for group D is 0.020 (recall the earlier remark that this is the most difficult group to integrate). The discrepancy in the group B can be traced to the fact that our integration program for the B diagram suffered from a computer overflow which forced us to exclude from the integration small regions of the integration domain. (The only other diagrams with the same problem were D and E; however, no discrepancy with the results of Sec. V arose in those cases.) Since there already exist analytical results for the group B, however, we have not attempted to resolve this difficulty. Replacement of ΔM_B by the analytic value of Ref. 8 changes (6.29) to

$$a_4^{(6)} = 0.910(30)\,, \tag{7.3}$$

which is in good agreement with the result of the approach of Sec. V.

We have also compared our integrals for individual diagrams with the results of Levine and Wright[11] and Levine and Roskies.[8] They are shown in Table V. The agreement is very good in general. Since we have not computed the fourth-order infrared integrals I_x, I_c, I_s, and I_l explicitly, we have not been able to compare all diagrams directly with the values of Refs. 8 and 11. Instead we have compared various combinations within which such fourth-order integrals cancel. We have not been able to compare our results with those of Ref. 12.

Note added in proof. Recently R. Carroll has shown us a diagram-by-diagram comparison (unpublished) of his results with those of Ref. 11. Individually they are all in good agreement. However, presumably because of the smaller number of integration points, numbers of Ref. 12 are consistently lower than ours.

ACKNOWLEDGMENTS

One of us (T.K.) would like to thank Dr. B. Zumino for the hospitality extended to him at CERN during the summer of 1973 where the major part of our numerical work was carried out. Thanks are due to the Japan Society for Promotion of Science and Dr. H. Miyazawa of the University of Tokyo where part of this work was done. We are indebted to Dr. R. F. Peierls of Brookhaven National Laboratory for generous support of our work in its early phase. We wish to thank Dr. A. Martin, Dr. L. van Hove, Dr. A. Peterman, Dr. J. Calmet, and Dr. H. Strubbe for their encouragement and helpful advice. The cooperation of the staffs of the CDC-7600 Computing Facility at CERN and computing facilities at Brookhaven National Laboratory, Cornell University, and SLAC is greatly appreciated.

APPENDIX: CALCULATION OF C_{ij}

Although (6.20) is adequate as a definition of C_{ij}, it is not convenient for actual calculation; in the sixth order there are 10 distinct C_{ij}'s for each electron self-energy diagram, and there are 10 terms in the defining summation for each C_{ij}. When (6.20) is evaluated explicitly, however, most terms are found to cancel each other. Thus a more convenient formula may be expected for C_{ij}.

A major simplification results from the use of formual (I.96) for the terms in (6.20):

$$B'_{ij}B'_{kl} - B'_{il}B'_{kj} = UB_{ij,kl}, \quad i \neq j \neq k \neq l \tag{A1}$$

where $B_{ij,kl}$ is given by (I.97), or the equivalent formula

$$B_{ij,kl}=\left(\frac{\partial^2 U}{\partial z_i\,\partial z_l}\right)^{-1}\left(\frac{\partial B_{ij}}{\partial z_l}\,\frac{\partial B_{kl}}{\partial z_i}-B_{il}\,\frac{\partial^2 B_{kj}}{\partial z_i\,\partial z_l}\right),\qquad i\neq j\neq k\neq l \quad \text{(A2)}$$

obtained from (A1) noting that $B_{ij,kl}$ does not depend on z_i, z_j, z_k, and z_l. Here i and l should not belong to the same chain, since the denominator vanishes otherwise.

If some indices of $B_{ij,kl}$ are identical, we can use an even simpler formula (I.101).

Further simplification follows from Kirchhoff's first law (I.44) for B_{ij}. Suppose we have

$$B_{im}-B_{jm}=B_{km}\ . \quad \text{(A3)}$$

Then we find by substitution in (6.20)

$$C_{im}-C_{jm}=C_{km}-\frac{1}{U}\sum_{l\in P^e} z_l B'_{lm}[\epsilon(i-l)-\epsilon(j-l)-\epsilon(k-l)]\ , \quad \text{(A4)}$$

where P^e is the continuous path of internal electron lines and

$$\epsilon(i-l)=\begin{cases}1, & i>l\\ 0, & i=l\\ -1, & i<l\ .\end{cases} \quad \text{(A5)}$$

Thus most C_{ij} can be expressed using some basic set of C_{ij} and $z_i B_{ij}/U$.

Let us now give some explicit examples of C_{ij}. No C_{ij} appears in the second-order self-energy diagram since it has only one fermion line. The simplest C_{ij} is found in the mass-insertion diagram 2* in Fig. 4(c). We find

$$C_{31}=z_7/z_{137}=A_1\ . \quad \text{(A6)}$$

C_{ij} in fourth order are still trivial to calculate; for diagram a, Fig. 4(c), we have

$$C_{21}=C_{31}=C_{32}=z_6z_7/U\ , \quad \text{(A7)}$$

and for diagram b, Fig. 4(c), we find

$$C_{21}=z_{37}z_6/U,\quad C_{31}=(z_7z_{26}-z_2z_6)/U,\quad C_{32}=z_{17}z_6/U\ . \quad \text{(A8)}$$

Sixth-order C_{ij} are not as compact. As an example let us give C_{ij} for the self-energy diagram H, Fig. 3. First, we calculate three "basic" C_{ij}

$$\begin{aligned}C_{21}&=[z_{36}z_7z_8+z_{345}z_6z_7+z_{34}z_5z_{67}+z_3z_4(2z_5+z_8)]/U\ ,\\ C_{31}&=-[z_2z_4(2z_5+z_{78})+z_2z_5z_{67}+(z_2-z_6)\,z_7z_8]/U\ ,\\ C_{32}&=[z_1z_4(2z_5+z_{78})+(z_1z_7+z_4z_6)\,z_{58}+z_6z_7z_8]/U\ ,\end{aligned} \quad \text{(A9)}$$

using (A2) and (I.101). The rest can be obtained by Kirchhoff's first laws:

$$\begin{aligned}C_{3j}-C_{2j}&=C_{5j}+(z_1B'_{1j}+z_4B'_{4j})/U\ ,\\ C_{3j}-C_{1j}&=C_{4j}-(z_2B'_{2j}+z_5B'_{5j})/U\ .\end{aligned} \quad \text{(A10)}$$

From (A9) and (A10) we find

$$\begin{aligned}C_{41}&=C_{31}+(z_2B_{12}+z_5B_{15})/U\ ,\\ C_{42}&=C_{32}+C_{21}-1+(z_2B_{22}+z_5B_{25})/U\ ,\\ C_{43}&=C_{31}+(z_2B_{23}+z_5B_{35})/U\ ,\\ C_{51}&=C_{31}-C_{21}+1-(z_1B_{11}+z_4B_{14})/U\ ,\\ C_{52}&=C_{32}-(z_1B_{12}+z_4B_{24})/U\ ,\\ C_{53}&=C_{32}-(z_1B_{13}+z_4B_{34})/U\ ,\\ C_{54}&=-C_{43}+C_{42}+1-(z_1B_{14}+z_4B_{44})/U\ .\end{aligned} \quad \text{(A11)}$$

C_{ij} for other self-energy diagrams of Fig. 3 can be obtained in the same fashion. They are usually simpler than the above example. This is especially true for diagrams with self-energy insertions, such as diagram A, Fig. 3.

---

*Work supported in part by the U. S. Atomic Energy Commission and by the National Science Foundation.

†John Simon Guggenheim Foundation Fellow.

[1]T. Kinoshita, Nuovo Cimento 51B, 140 (1967).

[2]J. Aldins, S. J. Brodsky, A. Dufner, and T. Kinoshita, Phys. Rev. Lett. 23, 441 (1969); Phys. Rev. D 1, 2378 (1970).

[3]S. J. Brodsky and T. Kinoshita, Phys. Rev. D 3, 356 (1971).

[4]T. Kinoshita and P. Cvitanović, Phys. Rev. Lett. 29, 1534 (1972).

[5]P. Cvitanović and T. Kinoshita, this issue, Phys. Rev. D 10, 3978 (1974).

[6]P. Cvitanović and T. Kinoshita, this issue, Phys. Rev. D 10, 3991 (1974).

[7]For a description of RIWIAD see, for instance, B. E. Lautrup, in *Proceedings of the Second Colloquium on Advanced Computer Methods in Theoretical Physics, Marseille, 1971*, edited by A. Visconti (Univ. of Marseille, Marseille, 1971).

[8]M. J. Levine and R. Roskies, Phys. Rev. Lett. 30, 772 (1973).

[9]K. A. Milton, W.-Y. Tsai, and L. L. DeRaad, Jr., Phys. Rev. D 9, 1809 (1974).

[10]Some individual diagrams have also been evaluated numerically. See A. De Rújula, B. E. Lautrup, and A. Peterman, Phys. Lett. 33B, 605 (1970); S. J. Brodsky and R. Roskies, *ibid.* 41B, 517 (1972); J. Calmet, University of Utah report, 1972 (unpublished).

[11]M. J. Levine and J. Wright, Phys. Rev. Lett. 26, 1351 (1971); Phys. Rev. D 8, 3171 (1973).

[12]R. Carroll and Y.-P. Yao, Phys. Lett. 48B, 125 (1974).

[13]J. Mignaco and E. Remiddi, Nuovo Cimento 60A, 519

(1969).
[14]J. Calmet and M. Perrottet, Phys. Rev. D 3, 3101 (1971).
[15]R. Barbieri, M. Caffo, and E. Remiddi, Nuovo Cimento Lett. 5, 769 (1972); D. Billi, M. Caffo, and E. Remiddi, *ibid.* 4, 657 (1972); R. Barbieri, M. Caffo, and E. Remiddi, *ibid.* 9, 690 (1974); R. Barbieri and E. Remiddi, Phys. Lett. 49B, 468 (1974); L. L. DeRaad, Jr., K. A. Milton, and W.-Y. Tsai, Phys. Rev. D 9, 1814 (1974).
[16]J. Calmet and A. Peterman, Phys. Lett. 47B, 369 (1973).
[17]C. Chang and M. J. Levine (unpublished).
[18]B. N. Taylor, W. H. Parker, and D. N. Langenberg, Rev. Mod. Phys. 41, 375 (1969).
[19]J. C. Wesley and A. Rich, Phys. Rev. A 4, 1341 (1971).
[20]S. L. Kaufman, W. E. Lamb, Jr., K. R. Lea, and M. Leventhal, Phys. Rev. Lett. 22, 507 (1969); T. W. Shyn, W. L. Williams, R. T. Robiscoe, and T. Rebane, *ibid.* 22, 1273 (1969); B. L. Cosens and T. V. Vorburger, *ibid.* 23, 1273 (1969).
[21]R. Vessot, H. Peters, J. Vanier, R. Beehler, D. Halford, R. Harrach, D. Allen, D. Glaze, C. Snider, J. Barnes, L. Cutter, and L. Bodily, IEEE Trans. Instrum. Meas. IM-15, 165 (1966).
[22]R. DeVoe, P. M. McIntyre, A. Magnon, D. Y. Stowell, R. A. Swanson, and V. Telegdi, Phys. Rev. Lett. 25, 1779 (1970); T. Crane, D. Casperson, P. Crane, P. Egan, V. W. Hughes, R. Stambaugh, P. A. Thompson, and G. zu Putlitz, *ibid.* 27, 474 (1971); J. F. Hague, J. E. Rothberg, A. Schenck, D. L. Williams, R. W. Williams, K. K. Young, and K. M. Crowe, *ibid.* 25, 628 (1970).
[23]A. Kponou, V. W. Hughes, C. E. Johnson, S. A. Lewis, and F. M. J. Pichanick, Phys. Rev. Lett. 26, 1613 (1971); J. Daley, M. Douglas, L. Hambro, and N. M. Kroll, *ibid.* 29, 12 (1972).
[24]The measurement of α by the ac Josephson effect is being improved right now (private communication from B. N. Taylor). [*Note added in proof:* The latest least-squares adjustment of the fundamental constants can be found in E. R. Cohen and B. N. Taylor, J. Phys. Chem. Ref. Data 2, 663 (1973)].
[25]We follow the notation and conventions of J. D. Bjorken and S. D. Drell, *Relativistic Quantum Fields* (McGraw-Hill, New York, 1965).
[26]S. J. Brodsky and J. D. Sullivan, Phys. Rev. 156, 1644 (1967).
[27]To avoid unnecessary complication we shall disregard the contribution from vacuum polarization loops throughout this paper except in Sec. I.
[28]The basic idea of this scheme is outlined in Ref. 3.
[29]M. Veltman, CERN report, 1967 (unpublished).
[30]P. Cvitanović, Cornell University Report No. CLNS-234, 1973 (unpublished); in *Proceedings of the Third Colloquium on Advanced Computing Methods in Theoretical Physics, Marseille, 1973,* edited by A. Visconti (Univ. of Marseille, Marseille, 1973).
[31]We wish to thank Dr. M. J. Levine for giving us a program which generates the integrands of Ref. 11.
[32]A. De Rújula, B. E. Lautrup, and A. Peterman, Phys. Lett. 33B, 605 (1970).
[33]Xerox copies of the FORTRAN program of ΔM_i for all diagrams are available upon request.
[34]The use of formulas like (6.4) leads us occasionally to IR-divergent integrals of the form $\int_0^1 x^3 dx/[x^2+\lambda^2(1-x)]^2$, which differ from the usual form $\int_0^1 x dx/[x^2+\lambda^2(1-x)]$ obtained by the $I_{G/S}$ operation of Sec. II by finite terms.